FAST Facility for Accelerated Service Testing

HTL High Tonnage Loop

An international, cooperative government-industry research program

FRA/ORD-91/18

FATIGUE DEFECT ORIGINATION AND GROWTH EXPERIMENT

DECEMBER 1991

U.S. Department of Transportation
Federal Railroad Administration
Washington, DC 20590

Association of American Railroads
50 F Street N.W.
Washington, DC 20001

RPI Railway Progress Institute
801 North Fairfax Street
Alexandria, VA 22314

NOTICE

This document reflects events relating to testing at the Facility for Accelerated Service Testing (FAST) at the Transportation Test Center, which may have resulted from conditions, procedures, or the test environment peculiar to that facility. This document is disseminated for the FAST Program under the sponsorship of the U. S. Department of Transportation, the Association of American Railroads, and the Railway Progress Institute in the interest of information exchange. The sponsors assume no liability for its contents or use thereof.

The FAST Program does not endorse products or manufacturers. Trade or manufacturers' names appear herein solely because they are considered essential to the object of this report.

ACKNOWLEDGEMENT

The authors wish to acknowledge Jon Hannafious, Roger Steele, and Bea Rael for their contribution to this report.

1. Report No. FRA/ORD-91/18	2. Government Accession No.	3. Recipient's Catalog No.
4. Title and Subtitle Fatigue Defect Origination and Growth Experiment		5. Report Date December 1991
		6. Performing Organization Code
7. Author(s) Paul Clayton (Professor) and Glenn Brave (Engineer)		8. Performing Organization Report No.
9. Performing Organization Name and Address Association of American Railroads Transportation Test Center P.O. Box 11130 Pueblo, CO 81001		10. Work Unit No. (TRAIS) 11. Contract or Grant No.
12. Sponsoring Agency Name and Address U.S. Department of Transportation Federal Railroad Administration Washington, D.C. 20590		13. Type of Report or Period Covered 1985-1987 14. Sponsoring Agency Code
15. Supplementary Notes		

16. Abstract

Between 1985-87 a number of different rail steels were tested at the Facility for Accelerated Service Testing (FAST) in the High Tonnage Loop using 100-ton capacity cars. Fatigue data on the formation of shells and detail fractures and growth rates of detail fractures were obtained.

The tendency of rail steels to form shells has been related to a parameter termed the Shell Index. This incorporates the volume fraction of oxide non-metallic inclusions, the tendency of those inclusions to form stringers, and rail hardness. The shell rate can be reduced by lowering the oxide content, reducing stringer formation, and increasing hardness. All three factors have to be considered in predicting rail steel behavior.

Under the specific test conditions employed, the crack propagation of detail fractures between 10 and 28 percent head area can be modeled by a linear function of million gross ton (MGT). The average growth rate for this size range was between 1.6 and 2 percent head area per MGT.

An investigation of the effect of lubrication level and high rail gage corner grinding on rail fatigue behavior proved to be inconclusive probably because of the narrow range of experimental conditions employed.

17. Key Words	18. Distribution Statement
Rail Steel Shell Detail Fracture Shell Index	This document is available through National Technical Information Service Springfield, VA 22161

19. Security Classification (of the report)	20. Security Classification (of this page)	21. No. Of Pages	22. Price

Form DOT F 1700.7 (8-72)

EXECUTIVE SUMMARY

The Fatigue Defect Origination and Growth Experiment was concerned primarily with rail fatigue behavior under 33,000 pound wheel loads in the Facility for Accelerated Service Testing (FAST) High Tonnage Loop under well lubricated conditions. After 150 MGT a large number of shells and detail fractures were produced.

The realization of the potentially large fuel savings that could be made from effectively lubricating the rail/wheel flange contact has led to more aggressive lubrication policies by railroads. A possible effect is, with wear heavily suppressed, fatigue will become the dominant life determining factor for rail. The major goal of the experiment was to better define the relationship between fatigue failures and the level of rail lubrication in curved track.

While the experimental plan worked, in that variation in the quantity of grease supplied to the different test segments was achieved, the degrees of dissimilarity in lubrication level were not enough to influence rail fatigue behavior.

One part of the experiment was to determine whether grinding the gage corner and gage side of the running surface of the high rail reduces the formation of shells and detail fractures. The only conclusion that can be drawn from the results is that the specific grinding pattern selected did not have any significant effect on rail fatigue. The effectiveness of rail grinding in controlling rail fatigue is still an open question as far as FAST data are concerned.

While these two aspects of the experiment have to be placed in a non-proven category, the results for two other areas were much more satisfactory. In the evaluation of rail metallurgy and cleanliness on fatigue initiation and determination of crack propagation rates of detail fractures, positive results were obtained.

A number of rail steels were tested in 5- and 6-degree curves. The rails were supplied by several manufacturers and differed in steel making practice, metallurgy and non-metallic inclusion content with some being in the head hardened condition. The tendency of the steels to form shells has been related to the parameter termed the Shell Index. This

incorporates the volume fraction of oxide non-metallic inclusion, the tendency of those inclusions to form stringers, and rail hardness. The incidence of shells can be reduced by lowering the oxide content, reducing stringer formation, and increasing hardness. All three factors have to be considered in predicting rail steel behavior.

While the Shell Index term is in the initial stages of development, it offers great encouragement to determine a definitive parameter which will enable future rail steel specifications to be based on fatigue performance.

The experiment differed from previous FAST experiments in that the train was run in a single direction in order to achieve different levels of lubrication around the loop. At 120.8 MGT, the procedure was changed slightly in that 30 dry down laps were carried out in the reverse direction every 3 MGT to prepare for ultrasonic testing . This was sufficient to produce marker rings on the detail fractures in track at the time and those that formed subsequently. This simple procedure made it possible to determine the rate of crack propagation in a number of detail fractures once they had been removed from the track and broken open.

Under the specific test conditions employed, the crack propagation of detail fractures between 10 and 28 percent of the head area can be modeled by a linear function of MGT. The average growth rate for this size range was found to be between 1.6 and 2 percent of the head area per MGT. While this information only applies to the FAST environment and cannot be directly applied to revenue service, it is extremely useful in helping to further improve the computer model being developed at the Volpe National Transportation Systems Center.

Table of Contents

Table of Figures

Tables

1.0 INTRODUCTION

Experiments carried out at the Facility for Accelerated Service Testing (FAST), Transportation Test Center, Pueblo, Colorado,[1] and in revenue service[2] have been very successful in demonstrating the large energy savings that could be achieved from effective wheel/rail lubrication. While this renaissance of lubricated operations has provided improvements in railroad economics, it raises the issue that, with wear heavily suppressed, fatigue will become the dominant life determining factor for rail.

Although the first three rail metallurgy experiments (RME) at FAST were carried out with a variety of steels and do not allow direct comparisons, qualitatively the results give a strong indication that fully lubricated running can lead to higher defect rates through sub-surface initiated fatigue.[3] A high defect rate was observed in RME II where the state of lubrication has been described as "over lubricated." In RME III the experimental conditions involved alternating periods of dry and lubricated running followed by 107 million gross tons (MGT) of fully lubricated operation. The defect occurrence was extremely low, even during the fully lubricated period. These results indicate a more complex interaction between fatigue and lubrication in which the prior history of the rail could have a significant effect on defect rates.

It is clear that there is a need to define the relation between fatigue failures and the state of rail lubrication in a more precise manner; particularly as railroads are implementing more aggressive lubrication policies. The major problem addressed by the FAST Fatigue Defect Origination and Growth Experiment was, therefore, the potential safety issue associated with fully lubricated operation in heavy curves.

At the same time the opportunity was taken to generate information that would enable the evolving models of rail fatigue initiation[4] and growth,[5] which are partly based on previous FAST results, to be tested.

2.0 EXPERIMENTAL DESIGN

To derive as much useful information as possible, and because of the intricately interwoven relations between wear, lubrication, metal flow, and fatigue, the experiments were designed to address a number of issues simultaneously.

1. *The effect of the degree of lubrication on fatigue:*

   The intention was to determine the effect of varying the level of lubrication, generated by a single lubricator under unidirectional running, on fatigue behavior throughout a 6-degree curve.

2. *The effect of gage corner grinding on fatigue:*

   The pioneering work of the Australians in reducing fatigue and wear in 2- and 3-degree curves by rail profile grinding suggests that this is one way to control fatigue in rails that are fully lubricated.[6] The purpose of this part of the experiment was to determine whether grinding the gage corner and gage side of the running surface of the high rail reduces the formation of shells and detail fractures by changing wheel/rail forces and contact locations.

3. *The effect of inclusion levels on fatigue:*

   A number of studies indicate that inclusions are a significant factor in the initiation of shells.[7,8,9,10] It was not practical to select rails with gradually increasing inclusion levels but, by including old standard carbon, new standard carbon and some specially prepared extra clean steels, it was anticipated that some new insights would be generated.

4. *The effect of rail metallurgy on fatigue:*

   RME II showed that harder rail steels provide greater resistance to fatigue.[11] New data were sought through incorporating into the experiment a variety of non-alloyed and low-alloy rail steels some of which were in the head hardened condition.

5. *The effect of wear rate on fatigue:*

   Current models of rail fatigue suggest that a certain amount of wear can help to control fatigue rates.[4] This particular issue has two aspects, namely, gage face and head height loss. The former was expected to be controlled to some extent by the level of lubrication whereas no direct control of the latter was attempted.

6. *The effect of track curvature on fatigue initiation:*

   The introduction of a 6-degree curve into the loop provided the opportunity to advance the understanding of the effect of curve radius on fatigue initiation beyond that of previous FAST experiments with 3- and 5-degree curves.

7. *The propagation rate of detail fractures in curved track:*

   A model of detail fracture crack propagation behavior has been developed based on previous FAST data from tangent track.[5] In the current experiment, the goal was to provide the first information from curved track to test the model.

The overall objective of the experiment was to acquire sufficient data to enable the above relationships to be better understood. The ultimate goal is to identify the best strategies for the economic control of rail defects. It would, however, be unrealistic to expect definitive data on all aspects from such a complex trial.

Although it would be desirable to incorporate inclusion volume fraction limits in rail specifications, the experiments reported here could at best be expected to offer guidelines for more specific tests in the future. Similarly, although rail grinding was investigated, only a single high rail ground profile was used without any accompanying low rail profiling. The experiments were not designed, therefore, to provide information on the broad spectrum of grinding practices.

Given the large number of rail steels and other conditions imposed on the experimental design, it was considered necessary to run the experiment for at least 150 MGT. To generate high tonnage more efficiently the old FAST loop was modified. For the first time the test track included a 6-degree curve enabling the test loop to be shortened from 4.78 miles to 2.77 miles creating the High Tonnage Loop (HTL). A further departure from previous operations was that the train was run predominantly in the counterclockwise direction, rather than by reversing direction every few days.

This report is concerned primarily with the sub-surface initiated fatigue behavior of the rail steels tested, but of necessity has to incorporate certain aspects of wear, lubrication, metal flow, and corrugation because of the interactive nature of these phenomena.

As with all FAST experiments, cost and timeliness considerations dictated that as many test variables as possible be included in the test plan. Given the statistical nature of fatigue, this requirement could threaten to compromise the scientific nature of the experiments. It will be shown in the body of this report, however, that the balance achieved was a reasonable one with much useful information being generated. Indeed, a good baseline has been developed to compare the performance of rails under heavier axle loads.

3.0 EXPERIMENTAL DETAILS

3.1 TRACK TESTS

Figure 1 is the layout of the FAST/HTL. The 5-degree curve of Section 03 has been used in all previous FAST experiments, but the new construction introduced a 6-degree curve for the first time.

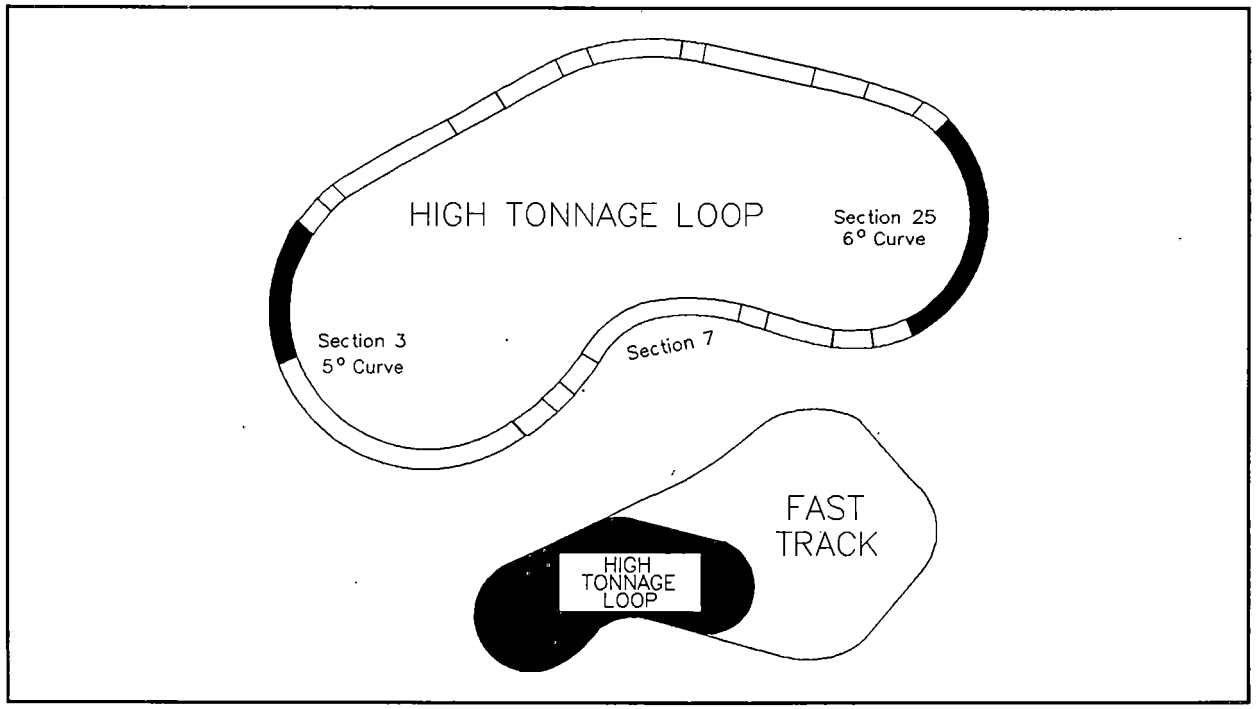

Figure 1. FAST/HTL Loop

General operation of the train throughout the test sections involved opening up to full throttle coming out of Section 07. The train entered Section 25 at 42 mph, but curve resistance reduced this to 38 mph before leaving the 6-degree curve. The speed through Section 03 was a constant 40 mph.

The train was made up of four locomotives and between 75 and 85 loaded 100-ton capacity cars. The train was run only in the counterclockwise direction for the first 120.8 MGT of the experiment. Subsequently the train was reversed every 3 MGT during the 30 dry down laps prior to ultrasonic testing (UT) of the rails. Train reversal generated detail fracture (DF) growth data by producing distinct growth ring markers at known MGT's.

The experiment was run with an unspecified mix of U and C wheel steels. At the start of the experiment, the vehicles retained the wheels employed in the previous FAST experiment -- RME III. The latter was conducted in the old FAST loop and the wheels were worn to a typical FAST profile. After about 5 MGT of running on the new HTL loop, those profiles had changed slightly to a new HTL standard worn wheel profile. This remained the stable pattern throughout the remaining 145 MGT of lubricated running. As the experiment progressed, wheels were gradually replaced because of wear but the percentage of new wheel profiles was always very low.

Comments concerning wheel profiles result from visual observations since no physical records of the transverse profiles were taken.

The rails covered by this report were located in Sections 03 and 25 (Figure 1). For the purposes of the experiment, Section 25 was divided into three segments, A, B and C, while only a part of Section 03 was included in the experimental layout.

The three lubricators employed in the experiment were all located on the outer rail so that lubrication protected the high rail in the test sections. The main lubricator was located in Section 24; the spiral leading into Section 25. With counterclockwise direction running, the degree of lubrication in Section 25 was expected to be greatest in Section 25A diminishing gradually through the 6-degree curve and being least in Section 03.

Trackside lubricators were supplied with the standard FAST grease, which has a calcium soap base and contains 12 percent graphite. Lubrication was always applied when required during the experiment. This was achieved by constantly monitoring and maintaining the main lubricator and by having a backup lubricator at the same location. Lubrication was deliberately interrupted for 30 laps of the train every 3 MGT to achieve dry rail conditions for regular ultrasonic testing of the track.

A third lubricator was used to quickly re-establish fully lubricated conditions following dry-down periods and at times when weather conditions hindered normal lubrication operations. At 90 MGT this auxiliary lubricator was moved from its original location in Section 26 to Section 01.

The state of lubrication in each of the four test segments was monitored by track inspectors every 0.1 MGT to 0.2 MGT using the TTC's Lubricant Level Gage (dubbed the goop gage - Figure 2). Typical measurements are recorded in Figures 3 a-d. While there are wide variations from one reading to the next for each segment, the general level of lubrication approached 30 in Section 25A, about 11 to 12 for Section 25B, 9 to 10 for Section 25C and 5 to 7 in Section 03. These numbers indicate that the aim of introducing variable lubrication, by the judicious use of carefully located lubricators, was achieved.

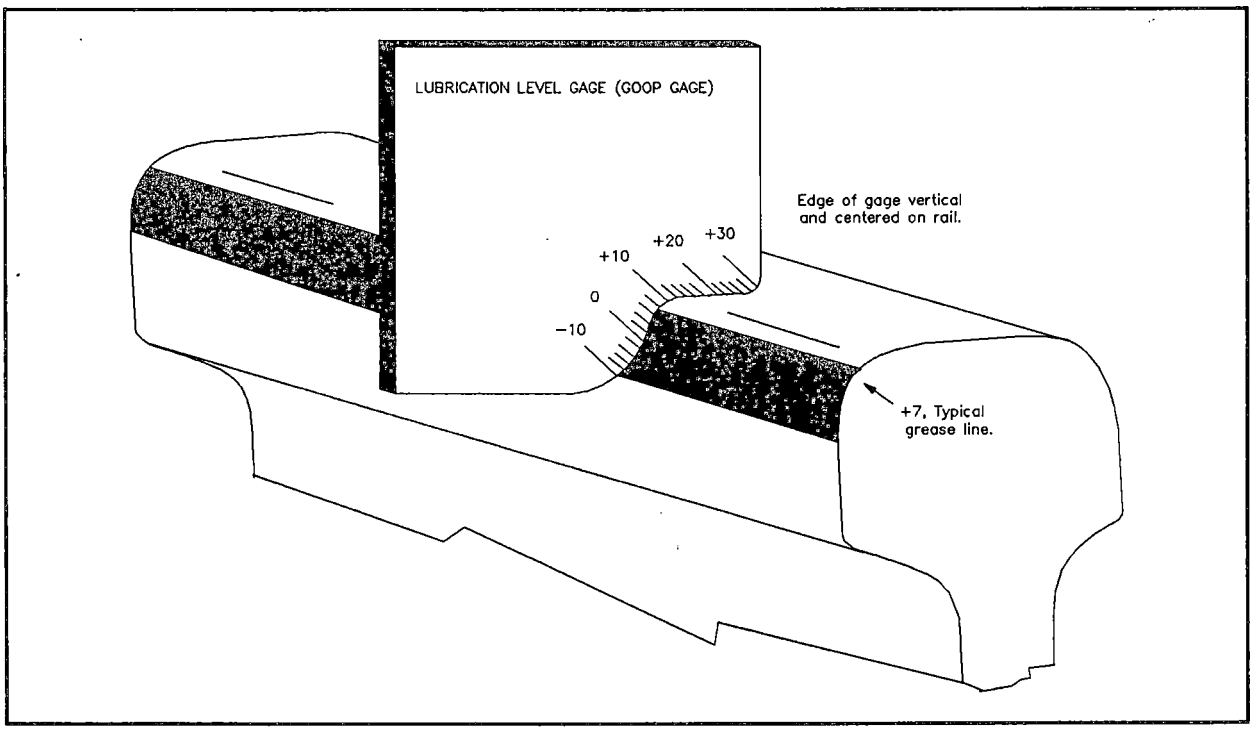

Figure 2. Gage Face Lubrication Measurement

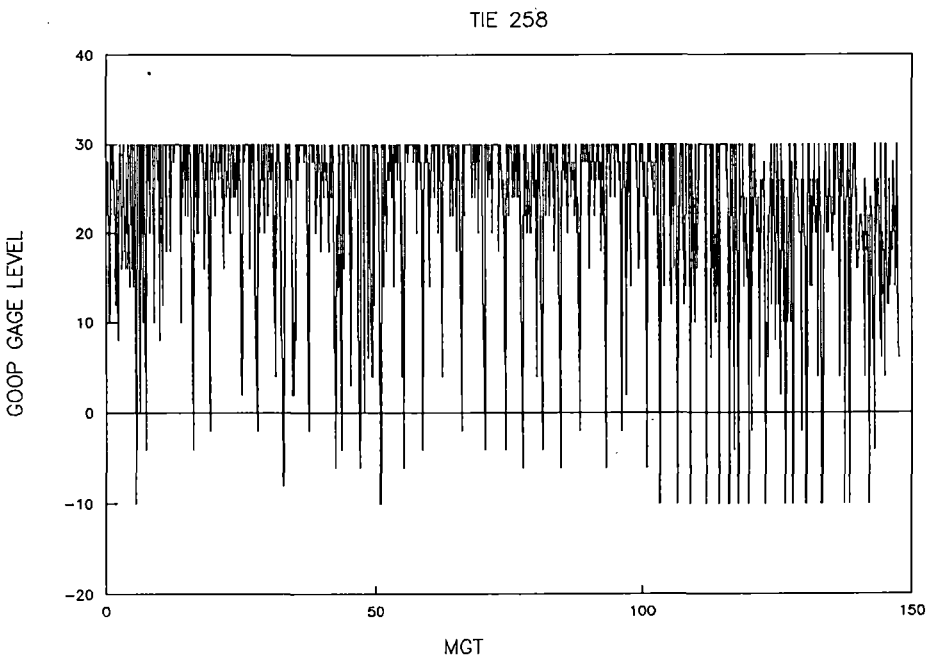

Figure 3(a). Typical Lubrication Level in Test Segment 25A

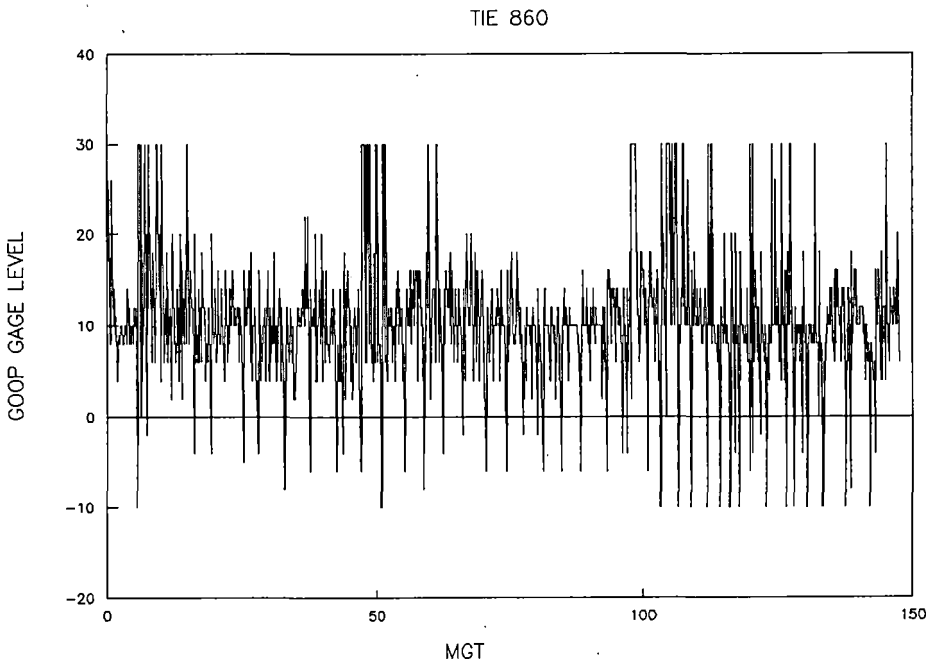

Figure 3(b). Typical Lubrication Level in Test Segment 25B

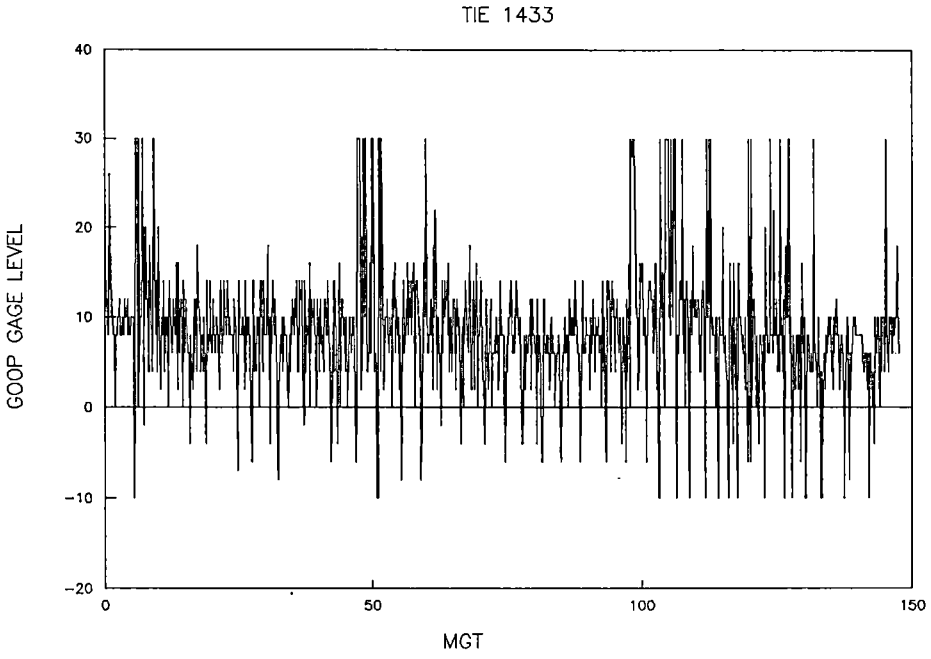

Figure 3(c). Typical Lubrication Level in Test Segment 25C

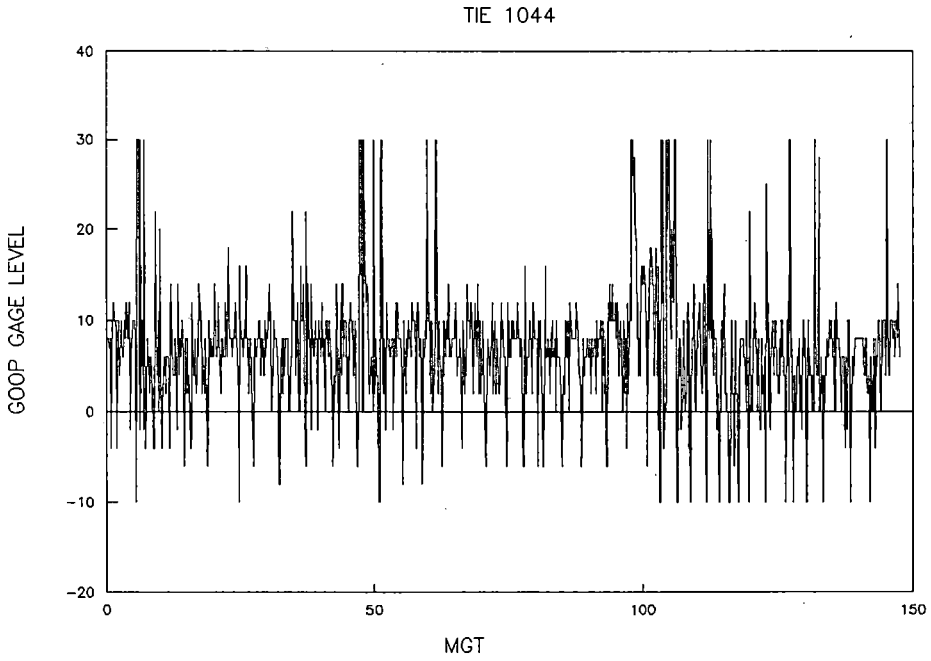

Figure 3(d). Typical Lubrication Level in Test Segment 03

Initially the inner rail was operated in the dry condition. Following a derailment at 90 MGT, the top of the inside rail was lightly lubricated with used motor oil applied by a modified vehicle mounted lubricator. The effects of this inner rail contamination are described by Heiss et al.[12]

Details of the four test segments are given in Figures 4a and b. The rail support conditions were similar in all four segments with the largest difference being that in Section 03 the ballast depth was 18 inches to 24 inches compared with only 12 inches in Section 25. Different rail steels were used from a number of rail manufacturers and grouped in different locations around the curves as evenly as availability would allow. Sections 25A and 25C were closely replicated to enable lubrication effects to be assessed.

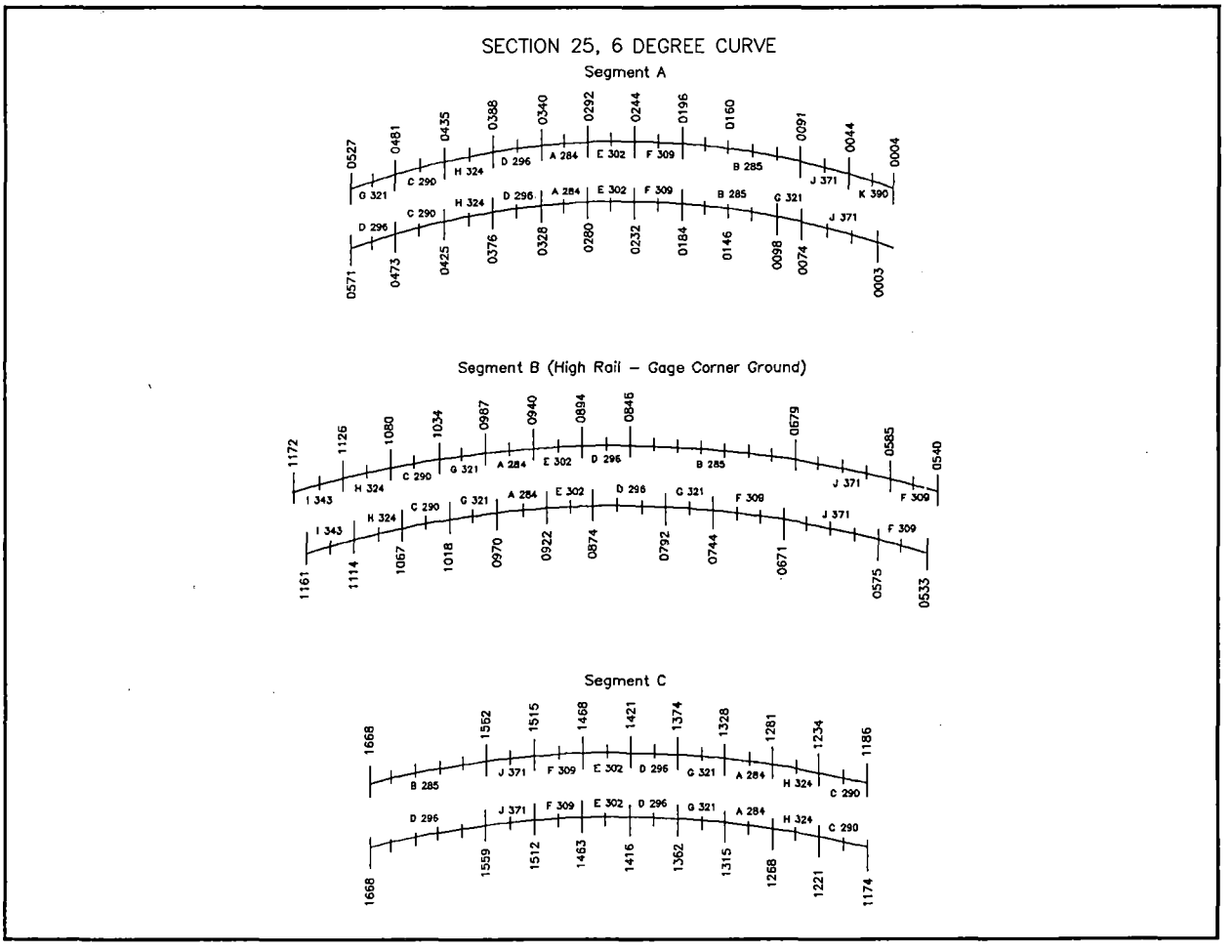

Figure 4(a). Rail Steel Layout and Tie Numbers for Section 25

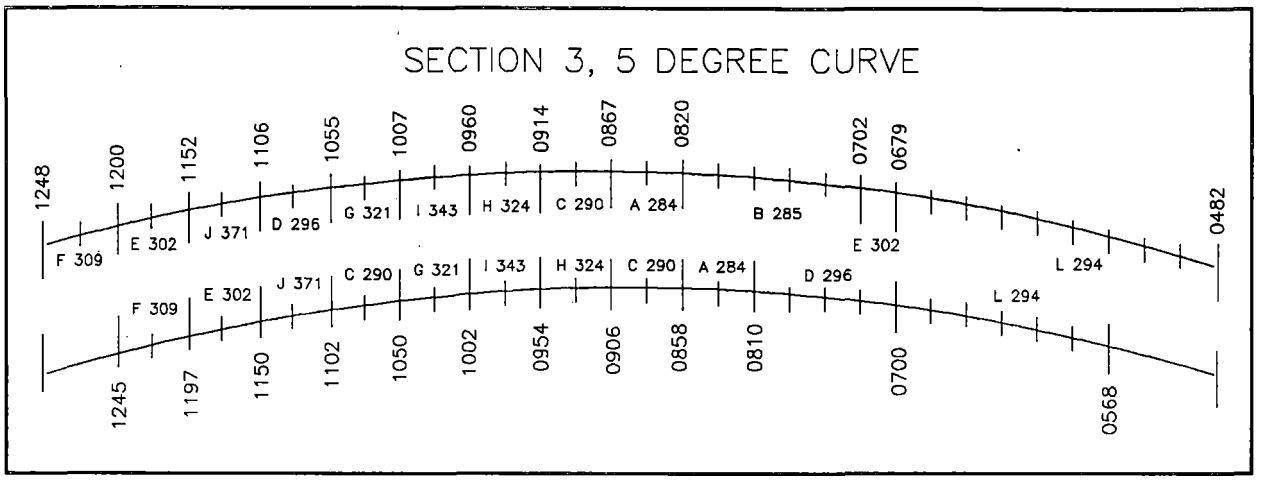

Figure 4(b). Rail Steel Layout and Tie Numbers for Section 03

The high rail in segment Section 25B was ground, before the experiment started, to the profile shown in Figure 5. The gage corner of the outer rail was re-ground at frequent intervals to maintain a profile which prevented normal wheel/rail contact on the gage corner. There were no plans at the outset to grind the top running surface of any of the test rails. However, it proved necessary to carry out rail top maintenance grinding of the inner rail and selected parts of the high rail during the course of the experiment.

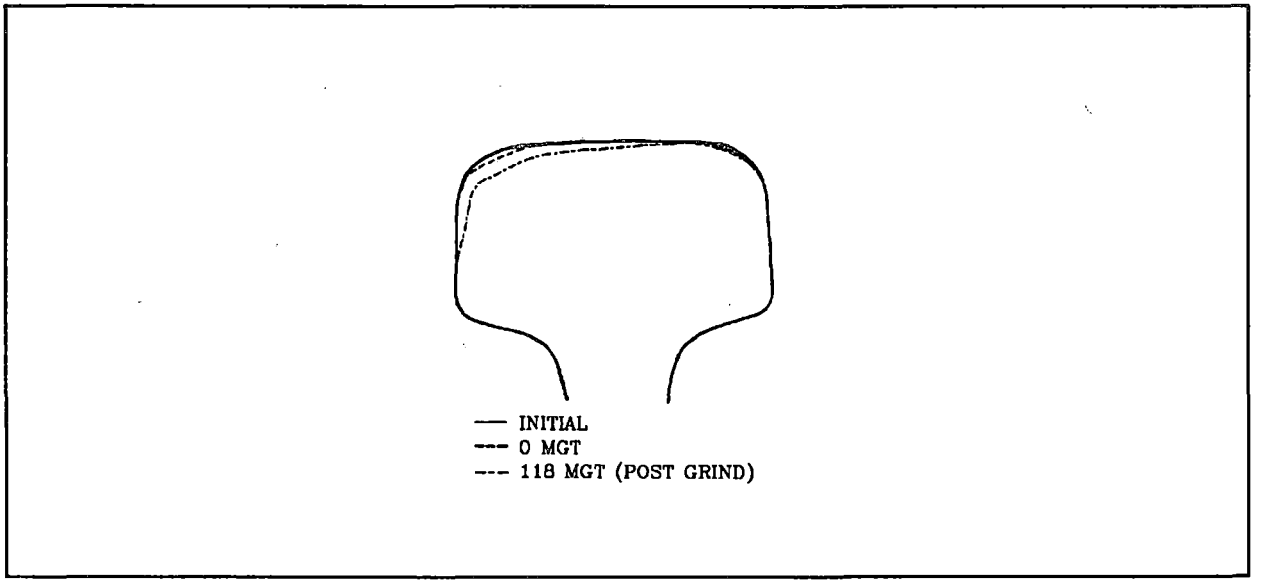

Figure 5. High Rail Profile Changes as a Result of Grinding and Wear in Section 25B

The general state of the track was monitored daily by track inspectors on foot, with a detailed track inspection every 3 MGT. An EM80 track geometry car was used to measure gage, superelevation, and rail alignment every 5 MGT. The criteria for corrective maintenance were based on the track geometry data and adherence to FRA class 4 track standards. At no time during the course of the experiment were any exceedances recorded in the test segments and corrective maintenance was not required. Apart from the grinding mentioned above, some maintenance was performed in Section 03 to restore superelevation, and an occasional low joint had to be corrected.

UT inspections were carried out every 3 MGT using the FAST R2 rail flaw detection vehicle which carried probes angled at 0 and 70 degrees to the rail vertical transverse plane. Any positive indications of a rail flaw were checked manually with a hand-held UT set. The size of the smallest detectable transverse defect was about 5 percent of the transverse rail head cross-sectional area. Any transverse defect of 10 percent or greater was protected with joint-bars. In some cases the joint-bars were loosely applied to allow defects to grow normally to 30 percent before the bolts were tightened.

The shells that formed early in the experiment did not receive full attention until they were hand-mapped and sized at about 50 MGT. Subsequent shell monitoring was carried out visually with an occasional session of UT mapping. Thus, no complete record of shell initiation and growth was developed. Two reasonably complete shell snapshots were obtained, however, at 90 and 150 MGT.

Wear data were collected at 33 MGT intervals with snap gages to give eight readings per 39-foot rail. On the high rail of the curves in Sections 03 and 25 head height loss and gage face wear at 3/8 inch and 5/8 inch from the top of the rail head were determined. At equivalent locations head height loss and metal flow was determined for the low rail. Transverse profiles were recorded at certain locations using the Yoshida rail profilometer.

No ambient temperature measurements were taken during the course of the experiment, but daily maximum and minimum temperatures were obtained from Pueblo airport records.

The neutral temperature of the rail was 95 degrees as installed. While every effort was made to maintain this value, it certainly would have been reduced at various times throughout the experiment as a result of plug insertions and seasonal variations.[13]

3.2 CHARACTERISTICS OF THE RAIL STEELS

The chemical composition and hardness of the rail steels used are given in Table 1. There are representatives of the old standard carbon, the new standard carbon, or intermediate strength (IS) steels, which contain about 0.2-percent chromium, and some low alloy steels. Rails J and K were head hardened.

Table 1. Chemical Composition of Rail Steels

RAIL	LABORATORY HARDNESS (Bhn)	C	Mn	Si	S	P	Cr	V
A	284	0.81	0.91	0.22	0.0002	0.014	0.03	0.00
B	285	0.75	0.85	0.17	0.0170	0.022	0.02	0.00
C	290	0.80	0.87	0.22	0.0050	0.017	0.02	0.00
D	296	0.75	0.91	0.36	0.0140	0.007	0.17	0.00
E	302	0.75	1.14	0.24	0.0150	0.012	0.19	0.00
F	309	0.80	1.12	0.40	0.0190	0.016	0.15	0.00
G	321	0.80	1.13	0.23	0.0190	0.018	0.19	0.00
H	324	0.79	0.93	0.44	0.0030	0.015	0.09	0.03
I	343	0.78	0.79	0.50	0.0060	0.024	0.41	0.06
J	371	0.85	0.91	0.22	0.0008	0.014	0.03	0.00
K	390	0.77	0.81	0.52	0.0050	0.023	0.42	0.06
L	294							

The hardness measurements were made in the laboratory with a Brinell hardness tester on transverse sections taken from used rail heads for all the rails except J and K. A pattern of indentations which avoided any of the surface work hardened layer was used (Figure 6). Hardness measurements on the two head hardened rails were made on unused rail with additional indentations. To ensure that these data were reliable the Brinell hardness tester was calibrated against test blocks of 205, 255 and 388 Bhn (Brinell hardness number). There was very little scatter in the hardness readings taken from any one rail steel.

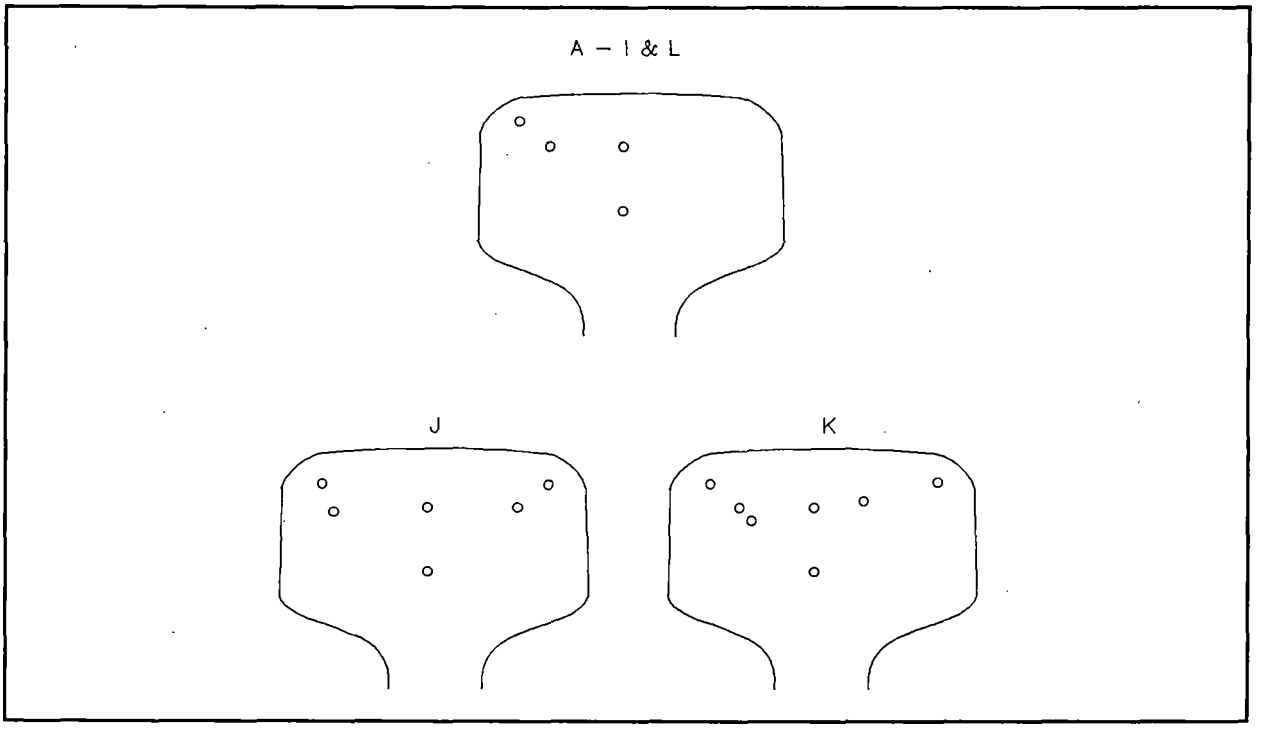

Figure 6. Location of Brinell Hardness Indentations

There was, however, considerable disagreement between the laboratory measurements and the rail surface measurements taken in the field in Section 25 with a portable King Brinell tester before train operation began (Table 2). Furthermore, King Brinell readings for Section 03 were much lower than those obtained in Section 25. Table 2 also shows the manufacturer's quoted hardness. In many cases there is a large discrepancy between this minimum guaranteed hardness and the one actually achieved. Unless otherwise stated all rail hardness values cited in this report are taken from the Brinell measurements made in the laboratory.

Table 2. Rail Hardness

RAIL	LABORATORY BRINELL	MANUFACTURER'S MINIMUM BRINELL	KING BRINELL
A	284	269	294
B	285	248	269
C	290	269	301
D	296	274	293
E	302	273	281
F	309	289	284
G	321	289	288
H	324	285	311
I	343	300	321
J	371		311
K	390		302
L	294	285	

Samples for non-metallic inclusion determinations were taken from selected rail steels at the approximate location at which shells are encountered, following Sugino et al,[14] (Figure 7). Measurements were carried out on the 10 x 20 mm (millimeter) horizontal plane highlighted in Figure 7.

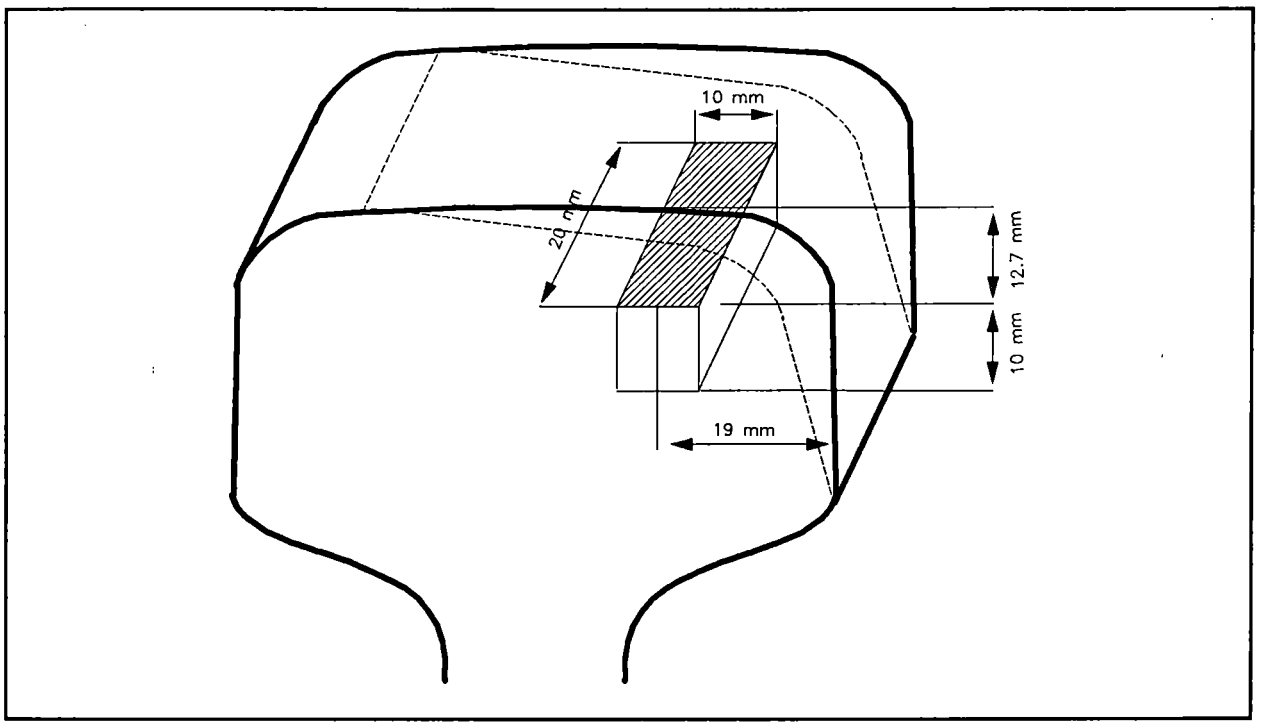

Figure 7. Location of Non-Metallic Inclusion Measurements

Sectioning was performed using liquid cooled abrasive cut-off saws. All specimens were mounted and ground using silicon carbide papers to a 15 μm (micrometer) finish. Polishing involved using a 2.5 μm diamond paste on a nylon cloth followed by a 0.03 μm alumina in a high pH sodium hydroxide solution on a neoprene chemical-polishing cloth. Each polishing step was performed at low speed and for the minimum amount of time required to produce an acceptable surface and retain the inclusions. To maximize the contrast between the inclusions and the microstructure, the specimens were not etched.

The volume fractions of oxide inclusions, Table 3, were measured in accordance with ASTM E542-83 using a 20 x 20 grid containing 400 points, with a spacing of 0.1 inch, at a magnification of 400x. This magnification and grid size provided an optimum relative size between the inclusions and the grid. A minimum of 30 fields was counted for each specimen.

Table 3. Inclusion and Shell Index Data

RAIL	HARDNESS	OXIDE VOLUME FRACTION (%)	STRINGER LENGTH μm	SHELL INDEX (-)
A	284	0.041	420	8.5
			380	
B	285	0.089	11700	4.4
C	290	0.004	980	10.3
			1060	
			100	
D	296	0.094	1030	6.8
F	309	0.051	100	9.8
G	321	0.033	1960	7.4
J	371	0.041	420	9.1
			380	

Oxide stringer measurements, Table 3, were made following the approach of Sugino et al[14] at a magnification of 100x in an optical microscope. Oxide stringers are defined by Sugino et al as clusters of alumina, 100μm or more in overall length, made up of individual globular inclusions separated by less than 100μm. The total oxide stringer length in the whole of the 200 mm^2 of surface was measured.

4.0 RESULTS

4.1 OVERVIEW

To understand the overall pattern of events during the experiment, it is necessary to have an appreciation of their chronological sequence. The following outline overview of the results can be best understood by referring to Table 4.

Table 4. Chronological Sequence of Main Events

MGT	EVENTS
0.0	Experiment started with wheel profiles worn to the old FAST worn profile, running only in the CCW direction. Inner rail bone dry and outer rail lubricated.
5.0	Wheels worn in to a new standard worn profile associated with the new HTL loop. These remained the dominant profile throughout the trial.
25.0	Corrugations appeared in the B 285 high rail in Section 25A.
50.0	Shells mapped for the first time with UT at certain locations.
59.6	First piece of B 285 removed from Section 25A because of shells.
61.7	Section 03 outer rail, 0750-0843, B 285 and A 284, ground.
68.9	First DF in Section 25B.
70.0	Corrugation obvious in Section 25B.
78.7	First DF in Section 03.
79.5	First DF in Section 25A. Section 03 outer rail, 0670-0820, B 285 and E 302, ground.
87.2	First DF in Section 25C.
90.0	Derailment. Inner rail ground, 0146-0184 B 285 Section 25A, 0328-0376 B 285 Section 25A, 0792-0874 B 285 Section 25B. All shells mapped. Inner rail lubrication commenced.
90.0	Vertical cracks from long shells to rail surface eliminated from the DF list.
96.1	Last B 285 removed from Section 25B.
100.0	Section 25C, Section 03 obvious corrugation. Last B 285 in Section 25A removed.
120.8	Dry down laps started in CW direction.
139.3	All of Section 03 and Section 25 inner rails ground.
150.0	HTL lubricated running terminated, old survivors removed from track while the last 10 MGT of the HTL experiment and the first 10 MGT of the HAL run.

Rail damage was seen as early as 25 MGT when the B 285 high rails of Section 25A corrugated. No corrugation measurements were taken and no quantitative data are available. Shells, which were associated with corrugations, appeared at about 35 MGT but were not documented until 50 MGT and for all four segments not until 90 MGT.

The first transverse defect was discovered at 68.9 MGT in Section 25B. The other segments experienced this defect within the next 20 MGT. Between 70 and 90 MGT there were so many closely spaced transverse defects detected by UT that the requirement to bar all such defects of 10 percent or more could no longer be met. This led to a decision to grind out and weld up a number of the defects. In the process of doing this, it was observed that some of the defects originated at the shell and propagated towards the surface of the rail, not into the rail head. This discovery led to a number of the recorded defects being re-classified and subsequent defects of this type not being recorded as DF's.

Although high rail corrugations, shells, and DF's were all present by 90 MGT, apart from the limited rail grinding carried out on the high rail in Section 03, the rails removed from the track and some work in Section 03 early on to adjust superelevation, there are no records of track deterioration leading to any specific track maintenance.

Beginning at 120.8 MGT, the 30 dry down laps, run every 3 MGT in preparation for UT, were carried out in a clockwise direction to provide marker rings on those transverse defects in existence at that time and those formed subsequently. This provided information on the growth rate of the transverse defects.

Throughout the experiment the low rail suffered from head crushing and metal flow resulting in all of the inner rails in the four test segments being given a full contour grind at 139.3 MGT.

4.2 TRACK GEOMETRY

The track geometry records from all four segments have been examined at 0, 60 and 90 MGT. They have been investigated with a view to answering the following questions:

1. Are there any obvious position in curve (PIC) effects such that the defect rate in any particular segment could be associated with features of the track geometry?
2. Are there any obvious PIC effects that might explain why any one segment experienced more track damage than another?
3. Did the corrugations in the B 285 rail steel lead to any obvious change in track geometry?

Figures 8(a-c) give examples of the track geometry output. Although it is difficult to draw firm conclusions from this type of plot (in that the interest is in specific features in a segment trace which shows considerable fluctuation irrespective of the parameter or segment involved) there is no apparent difference in the starting track geometries of the four different segments. In each case the superelevation was reduced with increasing MGT (in Section 03 superelevation was corrected) and the gage widened.

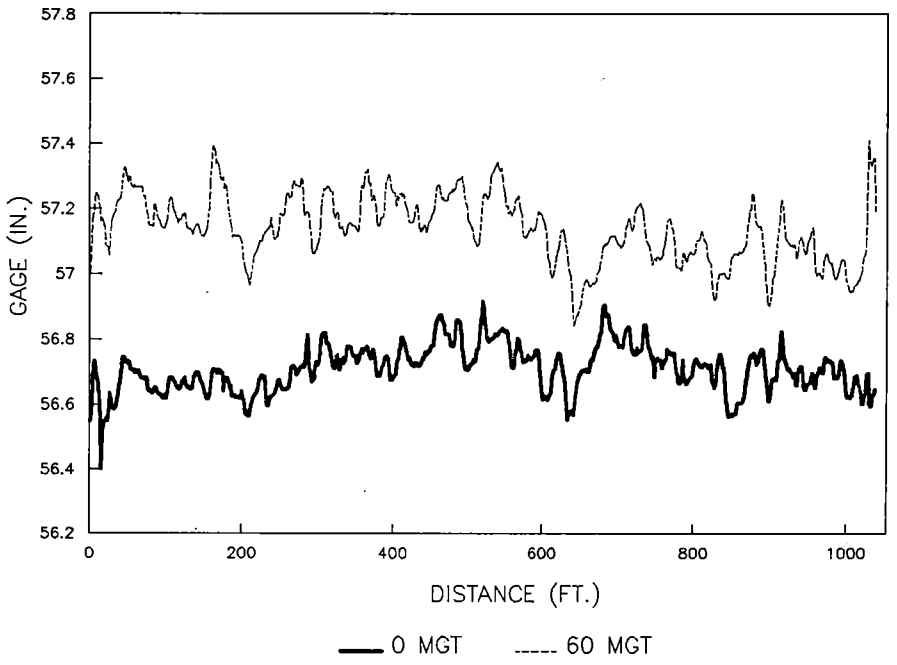

Figure 8(a). Example of Track Geometry Data for Section 25B -- Gage

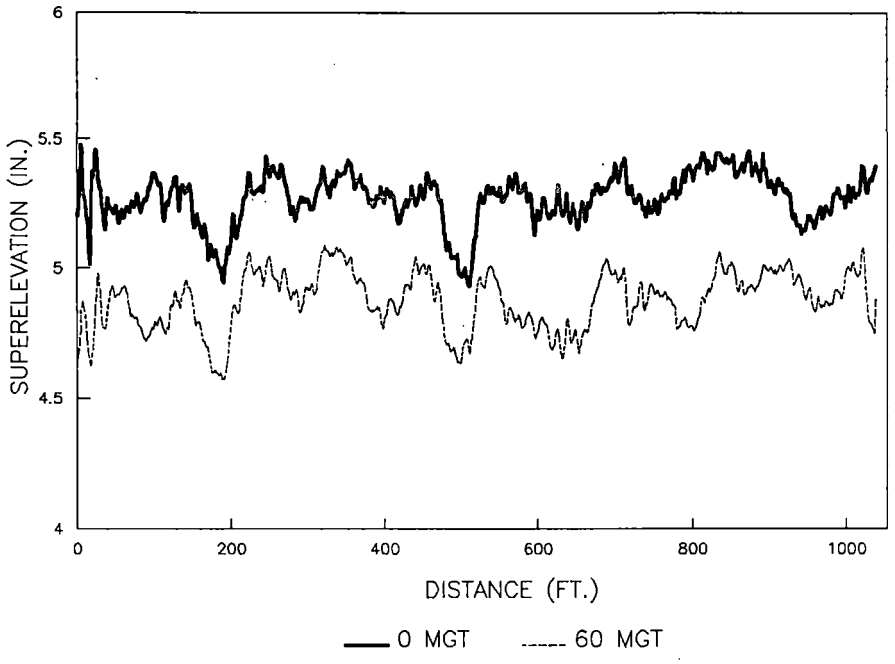

Figure 8(b). Example of Track Geometry Data for Section 25B -- Superelevation

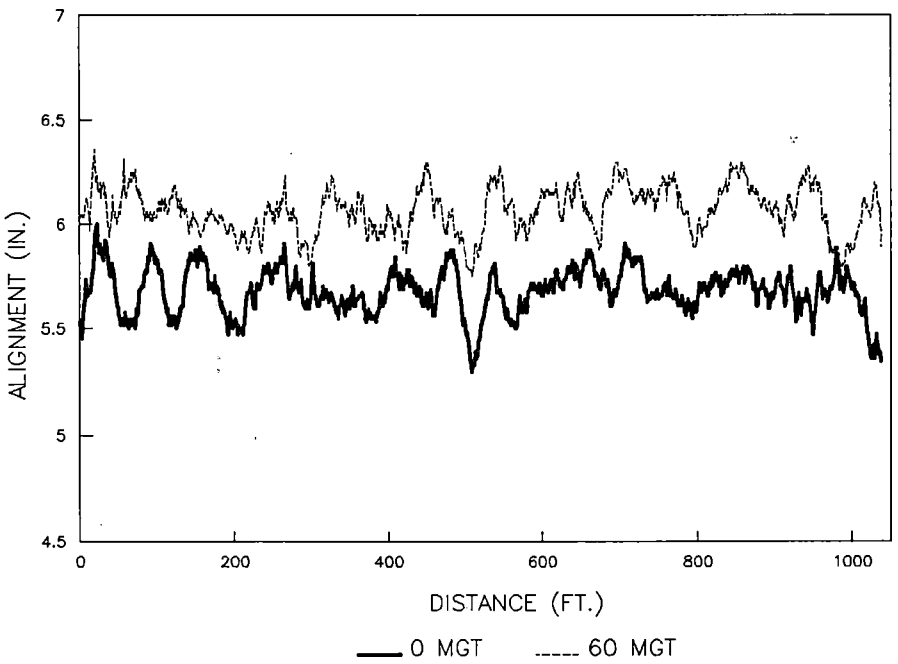

Figure 8(c). Example of Track Geometry Data for Section 25B -- Alignment

A detailed analysis of the outer rail alignment and the location of rail defects for the whole of Section 25 reveals that there was nothing unusual about the track geometry at locations which exhibited either a high defect rate or a very low one.

There is, therefore, no evidence to indicate a PIC effect of track geometry on the defect rate in the test segments. Furthermore, there was no evidence to suggest that the early corrugation of the B 285 rail led to any more track geometry deterioration than seen at other parts of the loop.

4.3 MAINTENANCE

A complete history of the overall maintenance records is not available. It has already been observed above, however, that there is no connection between rail corrugation or fatigue defects with track geometry maintenance requirements. A record of the rails removed from Sections 25 and 03 because of shell defects can be found in Tables 5(a-d), which records details of all shells that did not form DF's.

Table 5(a). Shell Data for Section 25A

	DEFECT LOCATION	METALLURGY	RAIL WT.	NO. OF SHELLS AT 90 MGT	AVG. LENGTH OF SHELLS	TOTAL RAIL REMOVAL MGT	NO. OF EXTRA SHELLS AT 150
1	0001-0023	K 390	132	0		178	
2	0023-0044	K 390	132	0		178	
3	0044-0067	J 371	136	1	0.75	178	
4	0067-0091	J 371	136	0		178	
5	0091-0115	B 285	136	12	7.54	59.6	
6	0115-0139	B 285	136	5	3.60	79.5	
7	0139-0160	B 285	136	10	3.68	100	
8	0160-0173	B 285	136	1	7.00	100	
9	0173-0196	B 285	136	15	2.98	100	
10	0196-0220	F 309	136	0		150	
11	0220-0244	F 309	136	0		150	
12	0244-0268	E 302	136	0		150	

Table 5(a). Shell Data for Section 25A -- (continued)

	DEFECT LOCATION	METALLURGY	RAIL WT.	NO. OF SHELLS AT 90 MGT	AVG. LENGTH OF SHELLS	TOTAL RAIL REMOVAL MGT	NO. OF EXTRA SHELLS AT 150
13	0268-0292	E 302	136	0		150	1
14	0292-0316	A 284	136	0		150	
15	0316-0340	A 284	136	0		150	
16	0340-0364	D 296	136	0		150	
17	0364-0388	D 296	136	0		150	
18	0388-0411	H 324	132	0		150	
19	0411-0435	H 324	132	0		150	
20	0435-0457	C 290	132	0		150	
21	0457-0481	C 290	132	0		150	
22	0481-0504	G 321	132	1	1.00	100	
23	0504-0527	G 321	132	7	3.82	100	

Table 5(b). Shell Data for Section 25B

	DEFECT LOCATION	METALLURGY	RAIL WT.	NO. OF SHELLS AT 90 MGT	AVG. LENGTH OF SHELLS	TOTAL RAIL REMOVAL MGT	NO. OF EXTRA SHELLS AT 150
1	0540-0561	F 309	136	0		178	
2	0561-0585	F 309	136	0		178	
3	0585-0608	J 371	136	0		178	
4	0608-0632	J 371	136	0		178	
5	0632-0655	J 371	136	0		178	
6	0655-0679	J 371	136	0		178	
7	0679-0702	B 285	136	14	3.61	96.1	
8	0702-0726	B 285	136	10	3.78	87.2	
9	0726-0750	B 285	136	3	5.33	96.1	
10	0750-0774	B 285	136	25	1.56	96.1	
11	0774-0798	B 285	136	57	1.89	96.1	
12	0798-0822	B 285	136	20	1.66	96.1	
13	0822-0846	B 285	136	12	1.81	96.1	
14	0846-0870	D 296	136	7	1.39	136	
15	0870-0894	D 296	136	3	1.00	136	
16	0894-0917	E 302	136	0		178	
17	0917-0940	E 302	136	0		178	
18	0940-0965	A 284	136	1	0.75	178	1
19	0965-0987	A 284	136	2	1.75	178	2

Table 5(b). Shell Data for Section 25B -- (continued)

	DEFECT LOCATION	METALLURGY	RAIL WT.	NO. OF SHELLS AT 90 MGT	AVG. LENGTH OF SHELLS	TOTAL RAIL REMOVAL MGT	NO. OF EXTRA SHELLS AT 150
20	0987-1010	G 321	132	0		178	1
21	1010-1034	G 321	132	2	0.50	178	
22	1034-1056	C 290	132	0		178	
23	1056-1080	C 290	132	0		178	
24	1080-1102	H 324	132	0		178	
25	1102-1126	H 324	132	0		178	
26	1126-1149	I 343	132	0		178	
27	1149-1172	I 343	132	0		178	

Table 5(c). Shell Data for Section 25C

	DEFECT LOCATION	METALLURGY	RAIL WT.	NO. OF SHELLS AT 90 MGT	AVG. LENGTH OF SHELLS	TOTAL RAIL REMOVAL MGT	NO. OF EXTRA SHELLS AT 150
1	1186-1210	C 290	132	0		150	
2	1210-1234	C 290	132	0		150	
3	1234-1257	H 324	132	0		150	
4	1257-1281	H 324	132	0		150	
5	1281-1304	A 284	136	0		130	
6	1304-1328	A 284	136	0		148	
7	1328-1356	G 321	132	0		148	
8	1356-1374	G 321	132	0		148	2
9	1374-1397	D 296	136	10	0.95	130	11
10	1397-1421	D 296	136	0		148	
11	1421-1444	E 302	136	0		178	
12	1444-1468	E 302	136	0		178	
13	1468-1491	F 309	136	0		178	
14	1491-1515	F 309	136	0		178	
15	1515-1537	J 371	136	0		178	
16	1537-1562	J 371	136	0		178	
17	1562-1583	B 285	136	1	1.75	132	1
18	1583-1608	B 285	136	5	2.15	132	1
19	1608-1632	B 285	136	1	8.25	132	9
20	1632-1656	B 285	136	1	0.75	132	3
21	1656-1668	B 285	136	1	4.50	132	3

Table 5(d). Shell Data for Section 03

	DEFECT LOCATION	METALLURGY	RAIL WT.	NO. OF SHELLS AT 90 MGT	AVG. LENGTH OF SHELLS	TOTAL RAIL REMOVAL MGT	NO. OF EXTRA SHELLS AT 150
1	0482-0506	L 294	132	0		178.0	
2	0506-0526	L 294	132	0		178.0	
3	0526-0546	L 294	132	0		150.0	
4	0546-0570	L 294	132	2	1.13	150.0	
5	0570-0590	L 294	132	0		150.0	1
6	0590-0614	L 294	132	0		150.0	2
7	0614-0638	L 294	132	0		150.0	
8	0638-0659	L 294	132	1	0.50	150.0	
9	0659-0679	L 294	132	0		150.0	
10	0679-0702	E 302	132	0		150.0	
11	0702-0726	B 285	136	2	6.50	87.0	
12	0726-0750	B 285	136	3	6.33	87.0	
13	0750-0774	B 285	136	1	0.25	150.0	
14	0774-0797	B 285	136	2	0.63	150.0	
15	0797-0820	B 285	136	10	4.75	66.0	
16	0822-0843	A 284	136	0		83.2	
17	0843-0867	A 284	136	8	0.64	127.2	
18	0867-0890	C 290	132	0		178.0	
19	0890-0914	C 290	132	0		178.0	
20	0914-0936	H 324	132	0		178.0	

Table 5(d). Shell Data for Section 03 -- (continued)

	DEFECT LOCATION	METALLURGY	RAIL WT.	NO. OF SHELLS AT 90 MGT	AVG. LENGTH OF SHELLS	TOTAL RAIL REMOVAL MGT	NO. OF EXTRA SHELLS AT 150
21	0936-0960	H 324	132	0		178.0	
22	0960-0983	I 343	132	0		150.0	
23	0983-1007	I 343	132	0		150.0	
24	1007-1031	G 321	132	0		178.0	
25	1031-1055	G 321	132	0		178.0	
26	1055-1083	D 296	136	0		178.0	4
27	1083-1106	D 296	136	0		167.0	
28	1106-1130	J 371	136	0		178.0	
29	1130-1152	J 371	136	0		178.0	
30	1152-1177	E 302	136	0		178.0	
31	1177-1200	E 302	136	0		178.0	
32	1200-1224	F 309	136	0		178.0	
33	1224-1248	F 309	136	0		178.0	

Table 6 lists the rail grinding operations carried out during the experiment and Figure 9 shows an example of low rail damage that prompted maintenance grinding.

Table 6. Rail Grinding Records

	MGT	I/O	TIE RANGE	METALLURGY
Sec 25	0	O	0540-1172	All Section 25B*
	25.05	O	0540-1172	All Section 25B
	40.40	O	0540-1172	All Section 25B
	61.71	O	0540-1172	All Section 25B
	79.53	O	0540-1172	All Section 25B
	90.08	O	0540-1172	All Section 25B
	90.08	I**	0146-0184	B285
			0328-0874	D296
			0792-0874	D296
	117.73	O	0540-1172	All Section 25B
	139.32	O	0894-1172	E302, A284, G321
				C290, H324, I343
	139.42	I**	0001-1668	All Section 25
	154.44	O	0540-1172	All Section 25B
Sec 03	61.74	O	0750-0820	B285, A284
	79.53	O	0670-0820	E302, B285
	139.32	I**	0568-1245	All Section 03

* Each Section 25B grind involved two passes
** Inner rail full contour grinding involved many passes

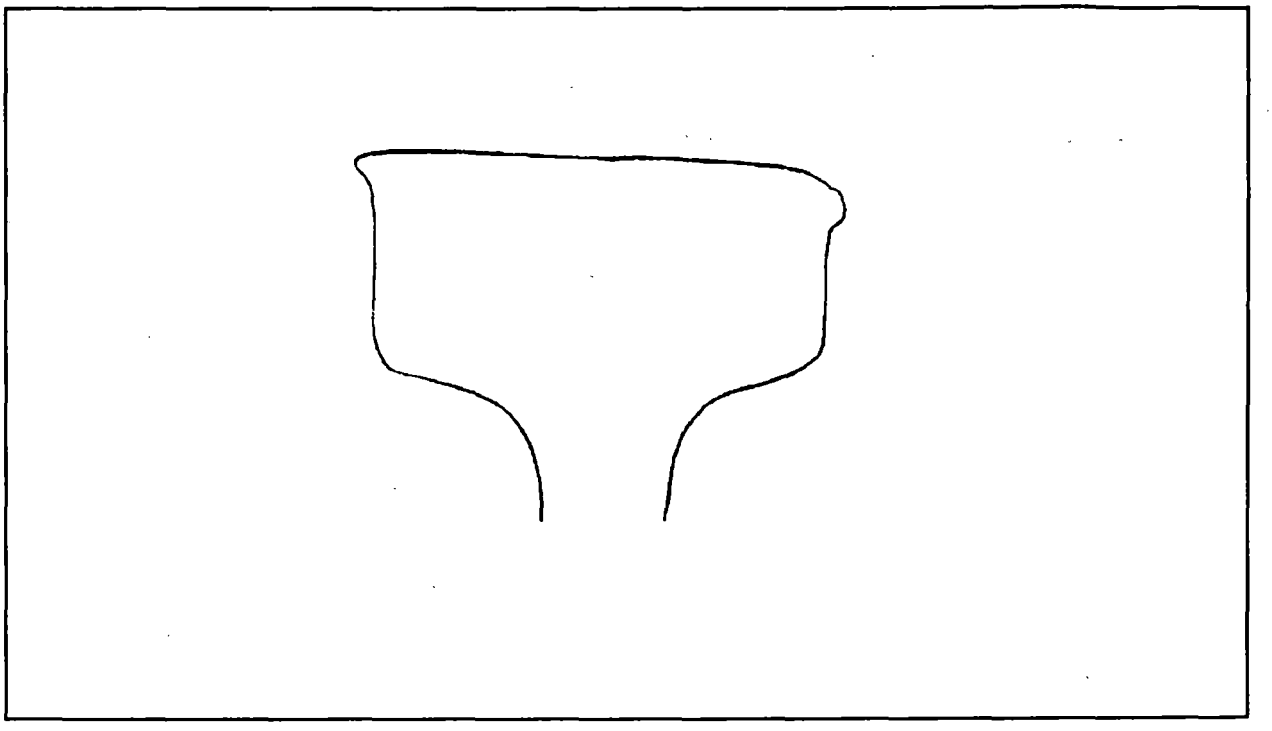

Figure 9. Typical Low Rail Transverse Profile before Maintenance Grinding

4.4 GRINDING PROFILE

The original ground profile given to the high rails in Section 25B and the way in which this profile changed with wheel contact and further grinding are shown in Figure 5.

4.5 WEAR DATA

The high rail head height (HH) and gage face (GF) wear rates for each metallurgy in the different test segments are given in Table 7 along with the GF:HH wear rate ratio where applicable. The head height loss data for the low rails are given in Table 8.

Table 7. Wear Rate for High Rails -- Inches Per MGT x 10^4

RAIL	S25A			S25B			S25C			S03
	HH	GF	GF/HH	HH	GF	GF/HH	HH	GF	GF/HH	HH
A284	17.5	22.9	1.3	23.8	60.0	2.5	17.3	25.8	1.5	39.7
B285	37.6			37.6	61.2	1.6	32.1	47.1	1.5	86.2
C290	15.3	20.1	1.3	22.5	59.5	2.6	11.9	17.3	1.5	16.7
D296	21.8	18.4	0.8	26.6	67.3	2.5	18.7	27.7	1.5	24.8
E302	10.2	45.1	4.4	17.9	62.1	3.5	15.6	44.5	2.9	15.1
F309	14.2	13.9	1.0	24.0	69.4	2.9	18.9	52.5	2.8	21.6
G321	15.3	25.0	1.6	23.4	77.3	3.3	12.3	36.9	3.0	19.9
H324	11.3	16.1	1.4	19.3	66.3	3.4	10.6	25.7	2.4	16.4
I343				16.3	78.4	4.8				8.5
J371										5.7

Table 8. Low Rail Head Height Loss
Inches Per MGT x 10^4

RAIL	S25A	S25B	S25C	S03
A 284	100.4	109.9	127.1	101.1
B 285	186.5		169.5	101.7
C 290	72.4	83.7	79.7	69.2
D 296	115.7	159.3	112.3	137.6
E 302	81.8	82.8	95.4	90.6
F 309	93.2	109.9	127.9	91.6
G 321	71.1	84.6	98.5	83.8
H 324	57.1	63.2	64.8	51.4
I 343		49.9		46.1
J 371	36.6	34.1	33.9	31.2

It is informative to consider the head height raw wear data and how the wear behavior of each individual steel has been determined for each segment of track. The head height measurements are plotted against MGT. The average wear rate (head height loss per MGT) for a particular metallurgy in any given segment is obtained from the best fit regression line through the combined data for that metallurgy.

Figure 10 shows one of the better plots of low rail head height loss in Section 25A. In general the low rail correlation coefficients were good, usually 0.9 or greater. The correlation was significantly worse for the high rails. Figures 11 and 12 provide examples of the best and worst cases respectively from Section 25A. The correlation coefficients for the high rail were often below 0.8.

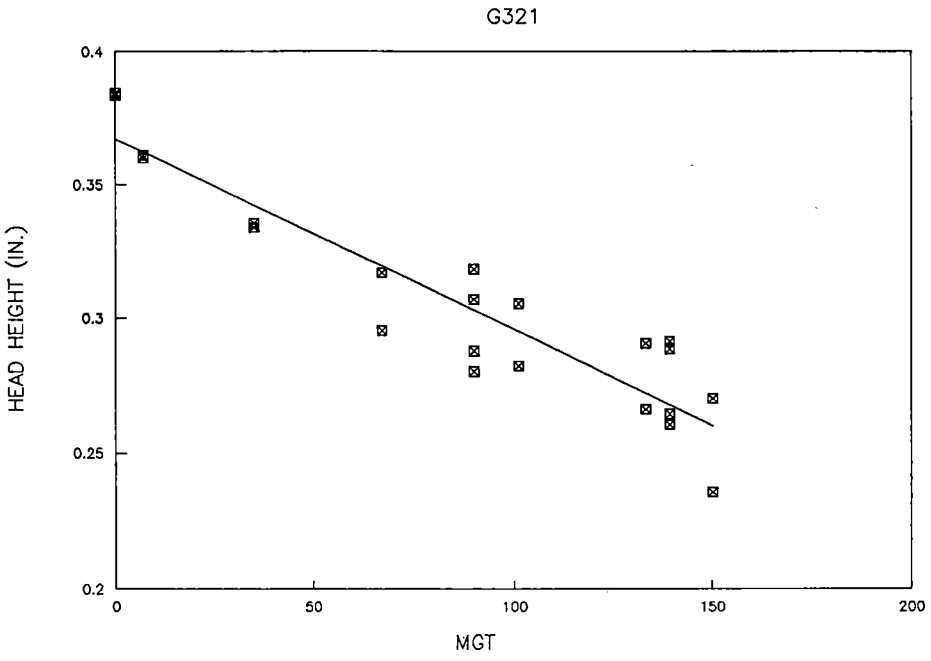

Figure 10. Low Rail Head Height as a Function of MGT; an Example of Good Correlation in Section 25A

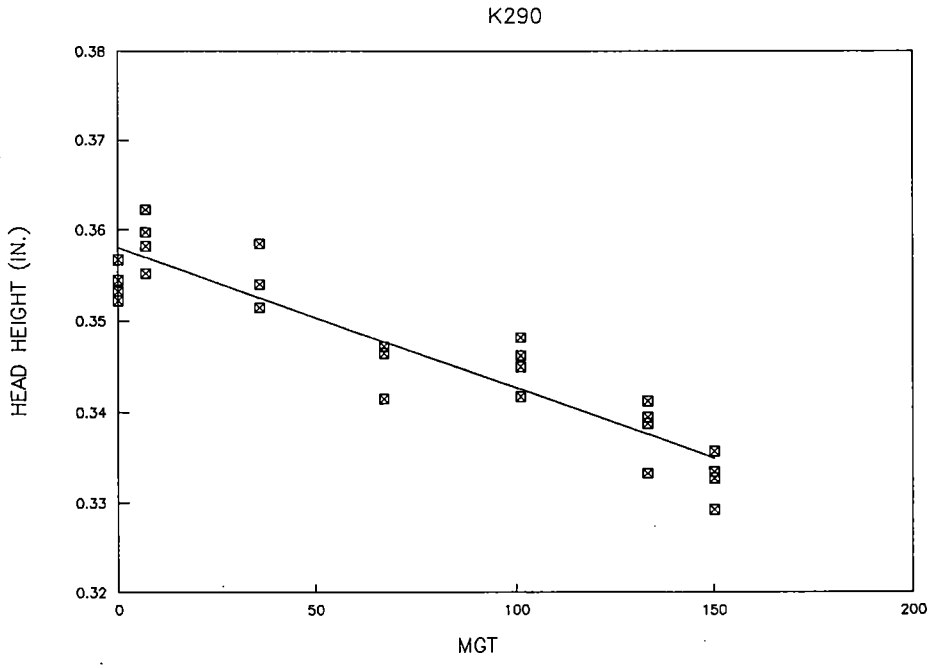

Figure 11. High Rail Head Height as a Function of MGT; an Example of Good Correlation in Section 25A

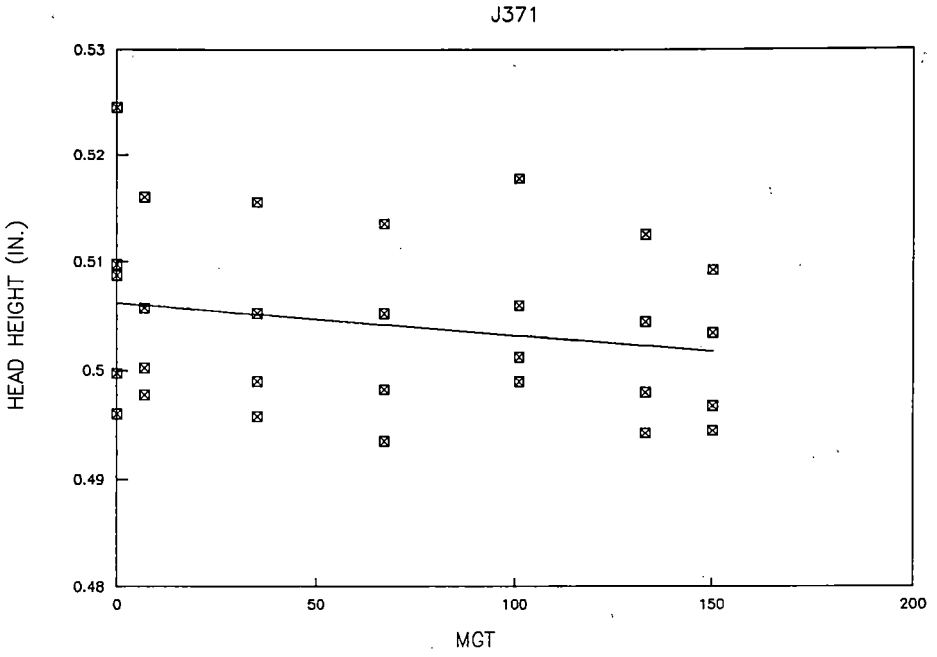

Figure 12. Low Rail Head Height as a Function of MGT; an Example of Poor Correlation in Section 25A

From Figure 12, it is apparent that much of the scatter results from the variation in the initial head height values. If this were to be removed by plotting head height loss against MGT the data points would be considerably consolidated. This also applies to the high rail gage face wear data which, in general, showed less scatter than the head height results.

In attempting to judge the PIC effects, the results for each individual rail metallurgy have to be considered (Table 7). The high rail wear rates in Section 25B were always higher than in Sections 25A or 25C, for all rail metallurgies. The wear rates in Sections 25A and 25C are in reasonably good agreement. There is, therefore, no indication of any influence of PIC on wear rates.

In Section 03 the head height wear rate of the high rail is always higher than in either Sections 25A or 25C. For two metallurgies, the rates in Section 03 are significantly higher than for Section 25B, but in all other cases they are slightly lower. The head height loss data for the low rails, Table 8, do not show the same pattern. Section 25C exhibits a head height wear rate that is often as high or higher than in Section 25B with the overall average head height loss in Section 03 considerably lower than in Section 25.

The GF:HH wear rate ratios for all the rail metallurgies, Table 7, are, in general, what would be expected from previous experience with lubricated track. As with the head height loss data, Section 25B also shows a higher gage face wear than either Sections 25A or 25C. It would appear, therefore, that the overall effect of the grinding in Section 25B has been to increase both head height and gage face wear.

In terms of the low:high head height rail wear rate ratios, Table 9, the pattern of behavior in Section 25B is again different to that in Sections 25A and 25C. The data in Table 9 are only for those rail steels which were installed in matched pairs on the high and low rail.

Table 9. HH Low:HH High Ratio for Matched Metallurgies

METALLURGY	S25A	S25B	S25C	S03
A 284	5.74	4.62	7.35	2.55
B 285	4.96			1.18
C 290	4.73	3.72	6.71	4.14
D 296	7.74		6.01	5.26
E 302	8.02	4.63	6.11	6.01
F 309	6.56	4.58	6.77	4.24
G 321		4.25	6.11	4.21
H 324	5.11	3.27	6.08	3.08
I 343		3.06		5.41
J 371	12.62	4.15	10.27	5.47
K 390				
L 294				3.81

4.6 SUBSURFACE INITIATED FATIGUE

The fatigue defects observed were shells, detail fractures, and vertical transverse cracks emanating from long shells. All the defects were, therefore, associated with the initiation of subsurface shells.

Although visual observations of shells were noted as early as 35 MGT, it was not until 50 MGT that even part of the test segments were documented by UT measurements. The only complete records of the shell population are at 90 MGT and the end of the experiment at 150 MGT. The history of the shell defects is, therefore, less than precise and certainly there is no information on the rate at which defects occurred as a function of MGT.

The 90 MGT data presented in Tables 5(a-d) are for shells which were either in the track at 90 MGT or had been in rails already removed from the test zones. The shell sizes were initially determined manually by UT. A number of the measurements were checked directly, after sectioning the rails. The general conclusion from this verification exercise was that UT tended to slightly overestimate the shell size but not enough to distort the general picture. The additional shells experienced by the rails remaining in track between 90 and 150 MGT are also shown in Tables 5(a-d).

A summary of the shells which did not form DF's is given in Table 10. In interpreting these data, it has to be recalled that there were different numbers of rails of each metallurgy in the high rail of each segment (Figure 4).

From Table 10, it would seem reasonable to conclude that the B 285 rail had dominated the results and that the grinding pattern imposed on the rails in Section 25B led to a higher number of shells than encountered in the other segments of the same curve. It must be emphasized, however, that given the small and variable rail sample sizes in any one segment, a superficial examination of the data could be misleading. For this reason the shell data are given further consideration in the Analysis section of this report.

Table 10. Summary of Shell Defects without DF's

RAIL		NUMBER OF SHELLS								TOTAL
		0-90 MGT				90-150 MGT				
		25A	25B	25C	03	25A	25B	25C	03	
A	284	0	3	0	8	0	3	0	*	14
B	285	43	141	9	18	*	*	17	*	228
C	290	0	0	0	0	0	0	0	0	0
D	296	0	10	10	0	0	0	11	4	35
E	302	0	0	0	0	1	0	0	0	1
F	309	0	0	0	0	0	0	0	0	0
G	321	8	2	0	0	*	1	2	0	13
H	324	0	0	0	0	0	0	0	0	0
I	343	-	0	-	0	-	0	-	0	0
J	371	1	0	0	0	0	0	0	0	1
K	390	0	-	-	-	0	-	-	-	0
L	294	-	-	-	3	-	-	-	3	6
					TOTAL:	53	160	49	36	298

* rails removed soon after 90 MGT
- steel not present at any time in this section

Specifics of each of the 51 DF's which occurred in the experiment are given in Table 11. The numbers for each segment at 90 and 150 MGT are summarized in Table 12. Only 13 DF's had been discovered by 90 MGT and only 6 of the 12 rail steels tested produced DF's. It is apparent that the occurrence of DF's is not purely a function of hardness.

Table 11. Detail Fracture History

LOCATION	RAIL	DISCOVERED		BARRED	REMOVED	
		SIZE (%)	MGT	MGT	SIZE (%)	MGT
Section 03						
03-0539	L 294	28	133.4		45	133.4
03-0541	L 294	30	150.2		30	150.2
03-0572	L 294	16	82.5	83.2	62	85.0
03-0572B	L 294	50	117.8		50	117.8
03-0576	L 294	26	150.2		26	150.2
03-0592	L 294	12	145.8	145.8	15	150.0
03-0658	L 294	38	127.2		38	127.2
03-0709	B 285	20	81.7	81.7	25	87.2
03-0775	B 285	2	98.4	105.2	41	111.0
03-0833	A 284	21	103.1		21	103.1
03-0834	A 284	14	79.5	79.5	47	87.2
03-0841	A 284	6	79.5	79.5	19	87.2
03-0847	A 284	13	81.7	82.5	35	87.2
03-0857	A 284	18	127.2		18	127.2
Section 25A						
25-0278	E 302	7	120.0		35	130.0
25-0279	E 302	8	137.2		33	141.8
25-0292	A 284	7	120.8		14	121.4
25-0293	A 284	10	112.0		18	121.4
25-0301	A 284	8	119.6		24	121.4
25-0307	A 284	5	149.8		9	150.0
25-0322	A 284	18	142.2	142.8	38	150.0
25-0329	A 284	18	79.5	79.5	43	87.2
25-0330	A 284	18	130.0		18	130.0
25-0484	G 321	41	85.0	85	50	87.2
25-0520	G 321				19	100.0
25-0499	G 321	26	123.1		36	124.1
25-0513	G 321	35	87.2	87.2	41	87.2

Table 11. Detail Fracture History -- (Continued)

LOCATION	RAIL	DISCOVERED		BARRED	REMOVED	
		SIZE (%)	MGT	MGT	SIZE (%)	MGT
Section 25B						
25-0681	B 285	6	68.9	75.3	53	79.5
25-0724	B 285	6	74.4	79.5	32	87.2
25-0858	D 296	32	87.2	87.2	50	88.2
25-0869	D 296	48	96.1		48	96.1
25-0873	D 296	21	117.7	188.8	42	124.1
25-0890	D 296	50	112.0		50	112.0
25-0945	A 284	13	87.2	87.2	59	103.6
25-0957	A 284	14	143.0	90.7	44	160.0
Section 25C						
25-1290	A 284	7	130.0		7	130.0
25-1294	A 284	38	90.9	90.9	38	91.0
25-1308	A 284	13	133.4	138.3	38	139.3
25-1316	A 284	11	141.0		39	147.8
25-1322	A 284	14	120.8		37	124.1
25-1341	G 321	21	117.7		34	120.8
25-1344	G 321	25	131.2	131.2	25	132.0
25-1352	G 321	33	112.0		33	112.4
25-1353	G 321	33	112.0		33	112.4
25-1354	G 321	25	112.0		25	112.4
25-1356	G 321	9	127.2		28	130.0
25-1359	G 321	10	133.4	138.3	38	139.3
25-1372	G 321	14	141.0		44	147.8
25-1385	D 296	28	87.2	87.2	38	87.2
25-1607	B 285	17	122.0		17	122.0
25-1654	B 285	6	117.7	122	22	122.0

Table 12. Summary of Detail Fractures

RAIL		NUMBER OF DETAIL FRACTURES								TOTAL
		0-90 MGT				90-150 MGT				
		25A	25B	25C	03	25A	25B	25C	03	
A	284	1	1	0	3	6	1	5	2	19
B	285	0	2	0	1	0	0	2	1	6
C	290	0	0	0	0	0	0	0	0	0
D	296	0	1	1	0	0	3	0	0	5
E	302	0	0	0	0	2	0	0	0	2
F	309	0	0	0	0	0	0	0	0	0
G	321	2	0	0	0	2	0	8	0	12
H	324	0	0	0	0	0	0	0	0	0
I	343	-	0	-	0	-	0	-	0	0
J	371	0	0	0	0	0	0	0	0	0
K	390	0	-	-	-	-	-	-	-	0
L	294	-	-	-	1	-	0	-	6	7
					TOTAL:	13	8	16	14	51

Note: The underlined data indicate that some or all of the rails were removed between 90 and 150 MGT.

Table 13, in presenting an average defect rate based on the number of starting rails, ignores the effect of rail removal during the experiment and does not indicate whether the defect rates were increasing or decreasing at 150 MGT. However, the results clearly reveal that the rails with the highest number of defects were A 284 and G 321, with not a single DF in the C,F,H,I J and K steels.

The total number of DF's in Section 25B was the same as in Section 03 (if L 294 is excluded); about half the number in Sections 25A and 25C. The incidence of DF's in the different segments and rail steels is covered in greater detail in the Analysis section.

Table 13. Average Defect Ratio Per Starting Rail

RAIL	NUMBER OF DETAIL FRACTURES
A 284	2.38
B 285	0.27
D 296	0.63
E 302	0.22
G 321	1.50
L 294	0.78

4.7 METALLURGICAL EXAMINATION OF DEFECTS

A number of the shells which developed DF's have been measured either visually or by UT in the laboratory (Table 14). Twelve of the DF's were opened up to reveal the cracks with their marker rings. Crack growth was determined as a function of MGT.

Table 14. Shell Dimensions

DEFECT LOCATION	TOTAL SHELL LENGTH (INCHES)	LENGTH BEFORE DF FORMED	SHELL WIDTH
03-0539	0.9	0.5	1.1
03-0541	1.2	0.9	0.9
03-0572B	1.3	0.8	0.9
03-0576	1.2	0.9	0.8
03-0592	1.8	1.1	1.1
03-0658	0.2	0.2	0.9
25-0279	0.1	0.1	0.5
25-0292	0.4	0.4	0.6
25-0293	2.3	1.5	0.9
25-0307	0.6	0.4	0.7
25-0322	1.1	0.8	0.9
25-0330	0.1	0.1	0.4
25-0499	1.3	0.8	0.9
25-0724	0.2	0.2	0.2
25-0890	1.6	1.3	0.9
25-1308	0.4	0.4	0.8
25-1316	0.3	0.3	0.5
25-1352	0.7	0.4	0.5
25-1354	0.4	0.2	0.6
25-1356	0.9	0.8	0.8
25-1359	0.9	0.6	0.9
25-1372	0.6	0.6	1.3
25-1654	0.7	0.7	0.9

In the B 285 rail, the shells occurred in association with corrugations. Although no detailed quantitative measurements were made, the corrugations were observed to be 6 to 12 inches in wavelength (Figure 13). A visual examination was carried out (Figure 14) to determine the spacial relationship between the shells and the corrugations. The conclusion reached was that the shells nearly always occurred in the troughs of corrugations.

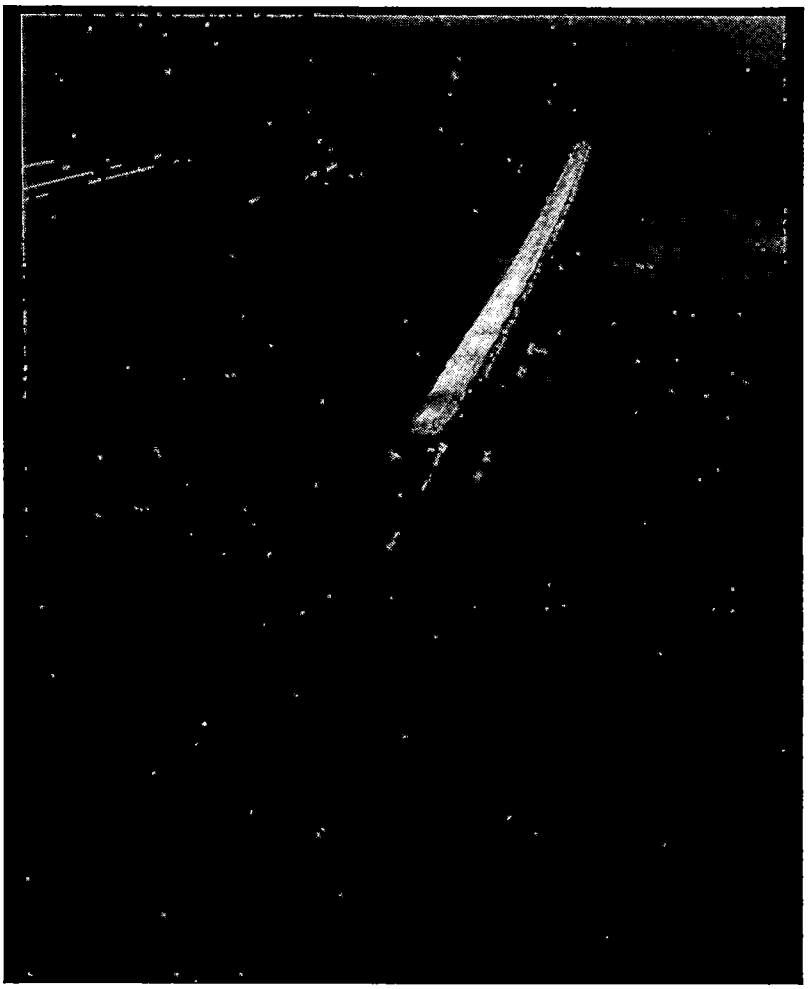

Figure 13. Corrugations in Rail B 285

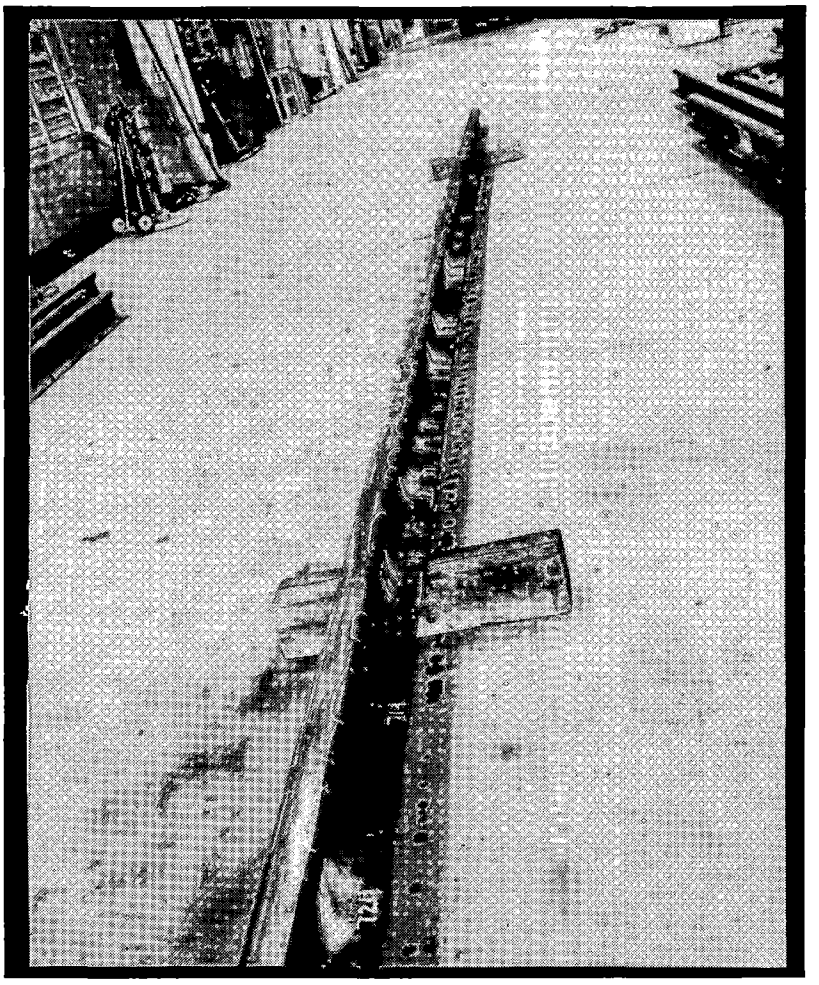

Figure 14. Spatial Relationship Between Shells and Corrugations in Rail B 285

From the DF's examined in the laboratory, it was found that the defects are typical of those reported previously (7-10). A thorough examination of one of the detail fractures, 25-0484, revealed that the relationship between the initiating shell and the transverse defect is also consistent with past findings.

Figure 15 shows a transverse section through defect 25-0484. The sectioning in this case has resulted in much of the transverse crack being destroyed but the drawn-in outline indicates the full extent of it. The orientations of the shell and the transverse crack can be seen better in the SEM photograph of Figure 16 with the shell details being revealed in Figure 17.

The central linear feature of the shell (Figure 17) is considered to be the initiation site of the defect. In this particular case it is about 4.25 mm long and 70μm high. It has been shown previously (7-10) that this step-like feature is usually associated with a stringer of oxide inclusions. A vertical transverse cross-section through the step shows (Figure 18) that there are indeed large oxide inclusions present in this case too.

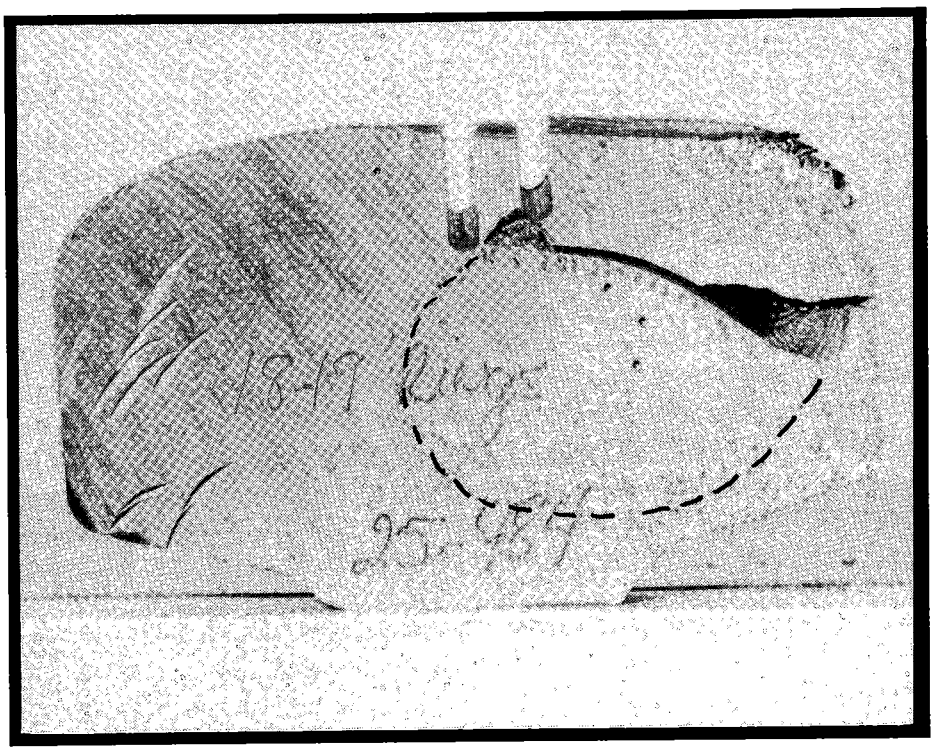

Figure 15. Transverse Section through Defect 25-0484

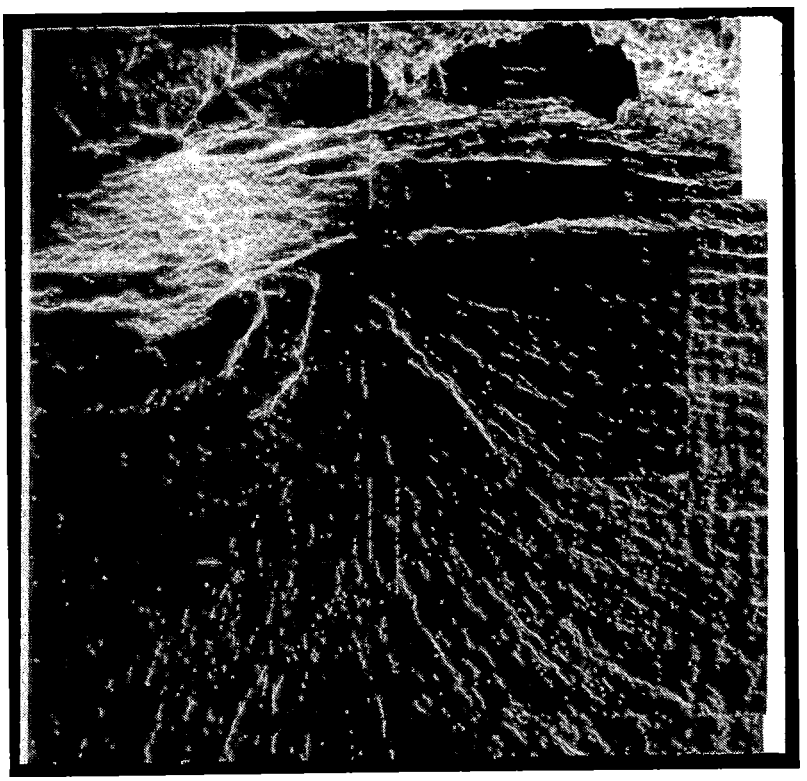

Figure 16. Transverse Defect Originating from Shell

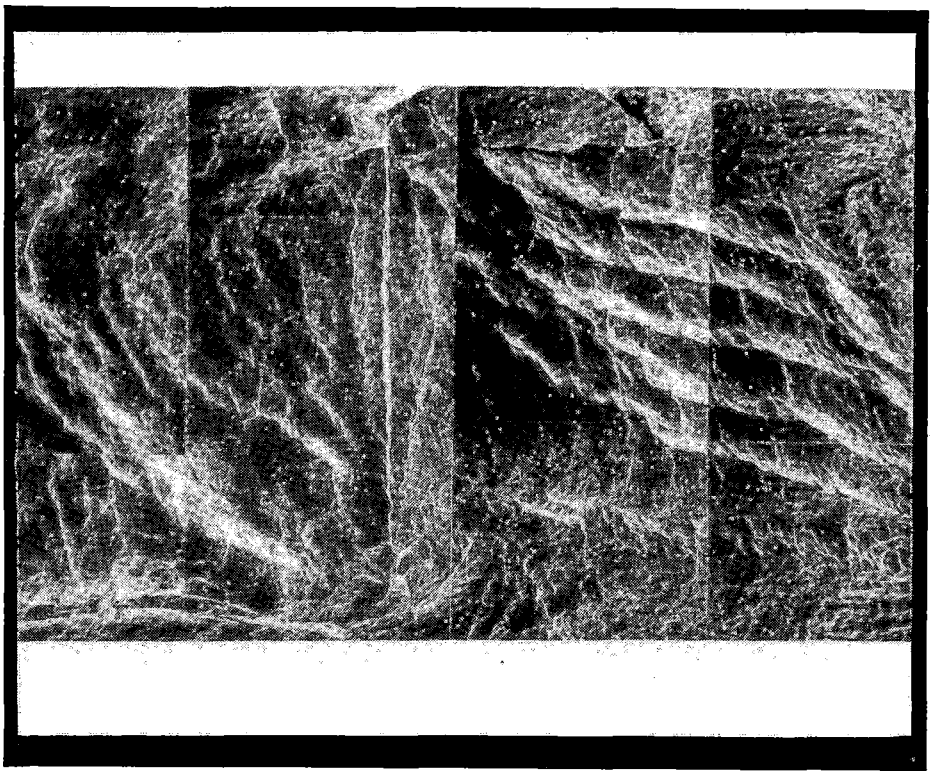

Figure 17. Top View of Shell Surface showing Initiating Step and Transition into DF

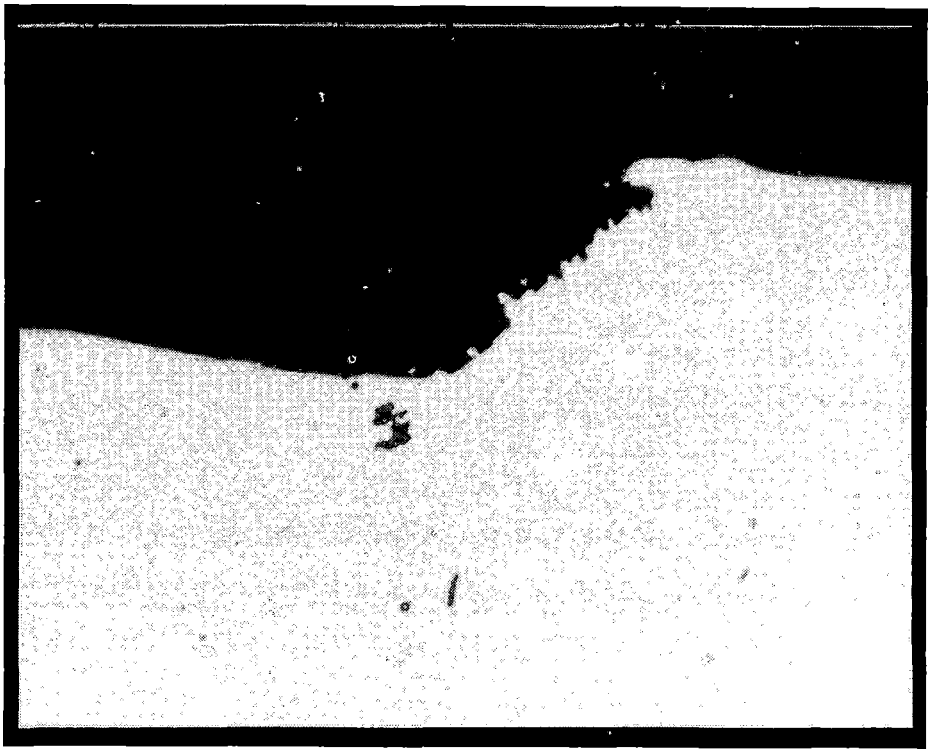

Figure 18. Transverse Cross Section through the Step in Shell of Defect 25-0484

The link between inclusions and a shell step was examined for other defects. Figure 19 shows a small shell, about 0.5 inch in diameter, from sample 25-7J. The step can be seen better in the close-up of Figure 20. Photographs taken with the SEM (Figure 21) and the optical microscope (Figure 22) reveal that there are numerous inclusion clusters at and near the step. Energy dispersive X-ray analysis indicated (Figure 23) that the inclusions are probably alumino-calcium silicates.

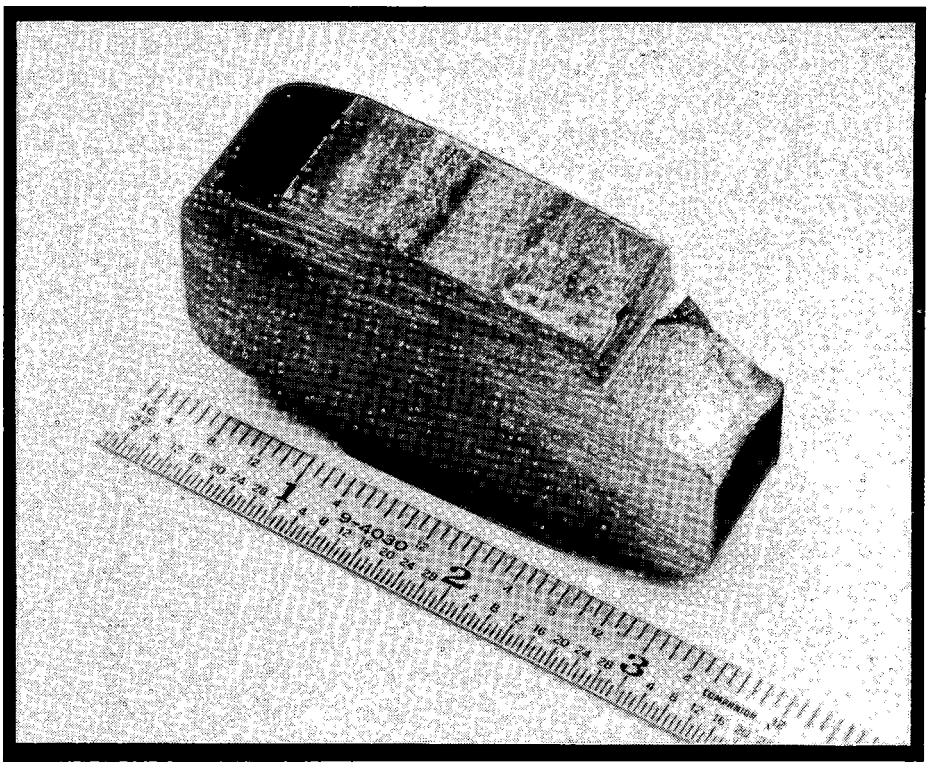

Figure 19. Small Shell in Sample 25-7J

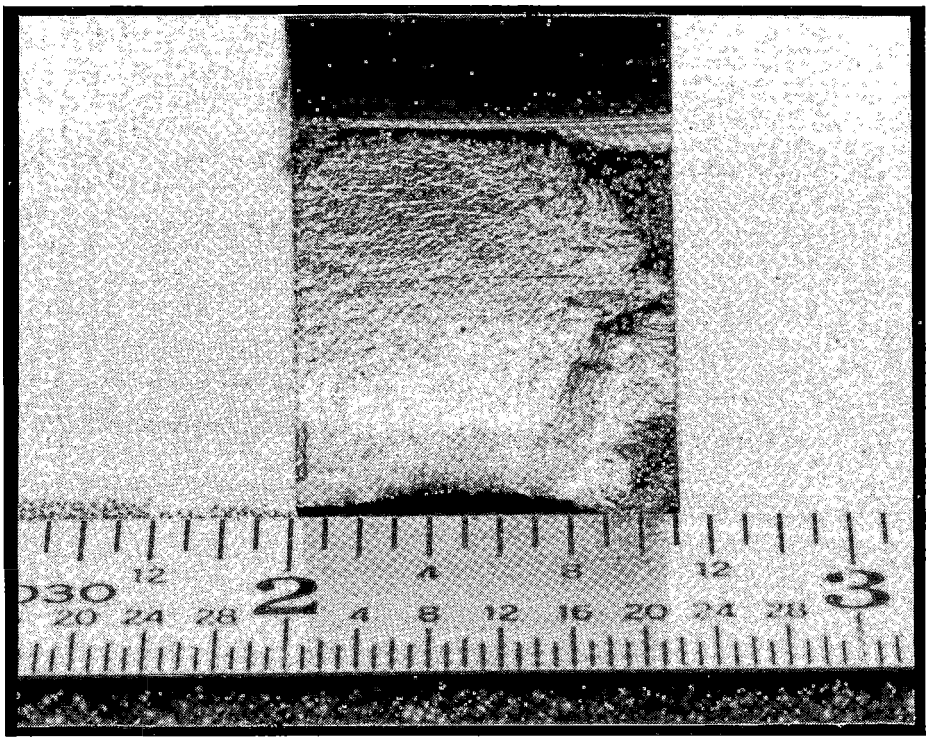

Figure 20. Step Feature in Shell from 25-7J

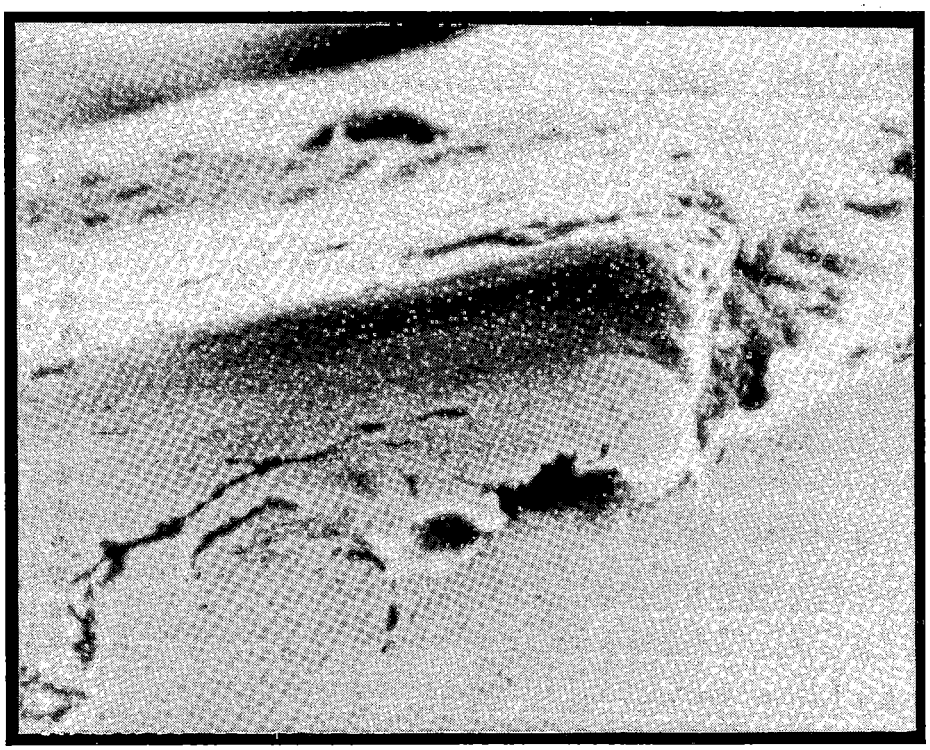

Figure 21. Scanning Electron Micrograph of Transverse Section through Shell in Figure 20

Figure 22. Optical Micrograph of Transverse Section through Shell in Figure 20

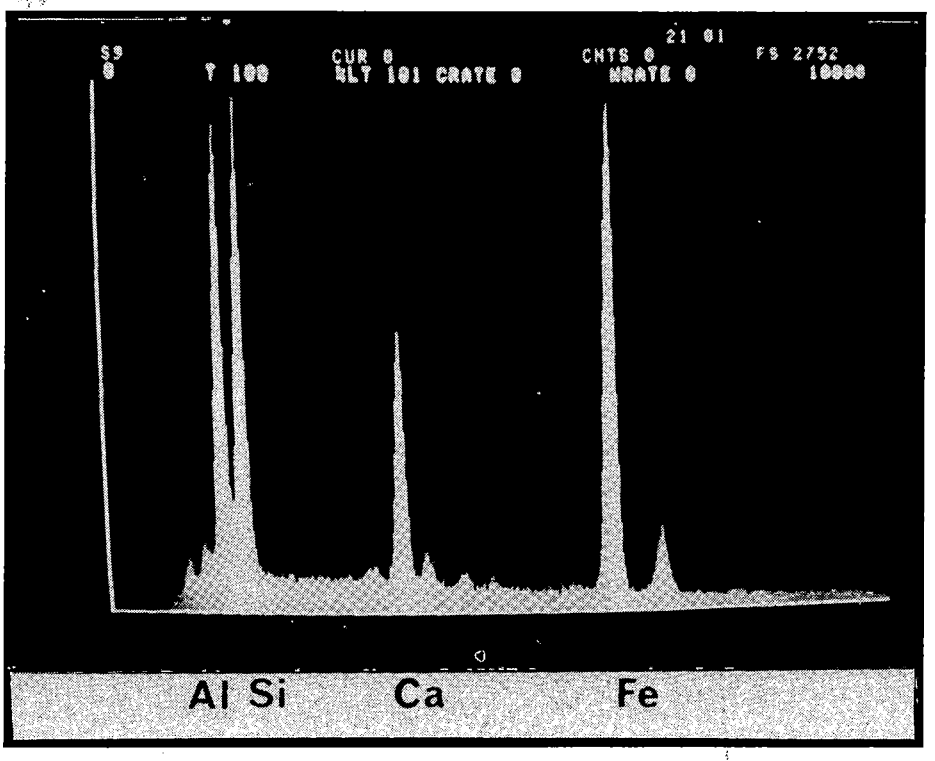

Figure 23. Energy Dispersive Spectrography Analysis of Inclusions Asssociated with Shell in Figure 20

The shells in Section 25B were somewhat different from any that have been reported previously in that they propagated on two planes (Figure 24). The relationship of the orientation of the two planes to the ground profile strongly indicates an influence of gage corner grinding on shell appearance. The batter of the crack face, in this particular case, prevents any observations of the initiating step. An example of a detail fracture initiated by a bi-planar shell is seen in Figure 25.

A notable feature of the shell investigation was that some very small shells were observed. Figure 26 shows one example near a defect at location 25-0105. The shell has a distinct central step feature and is only about 6 mm long (Figure 27).

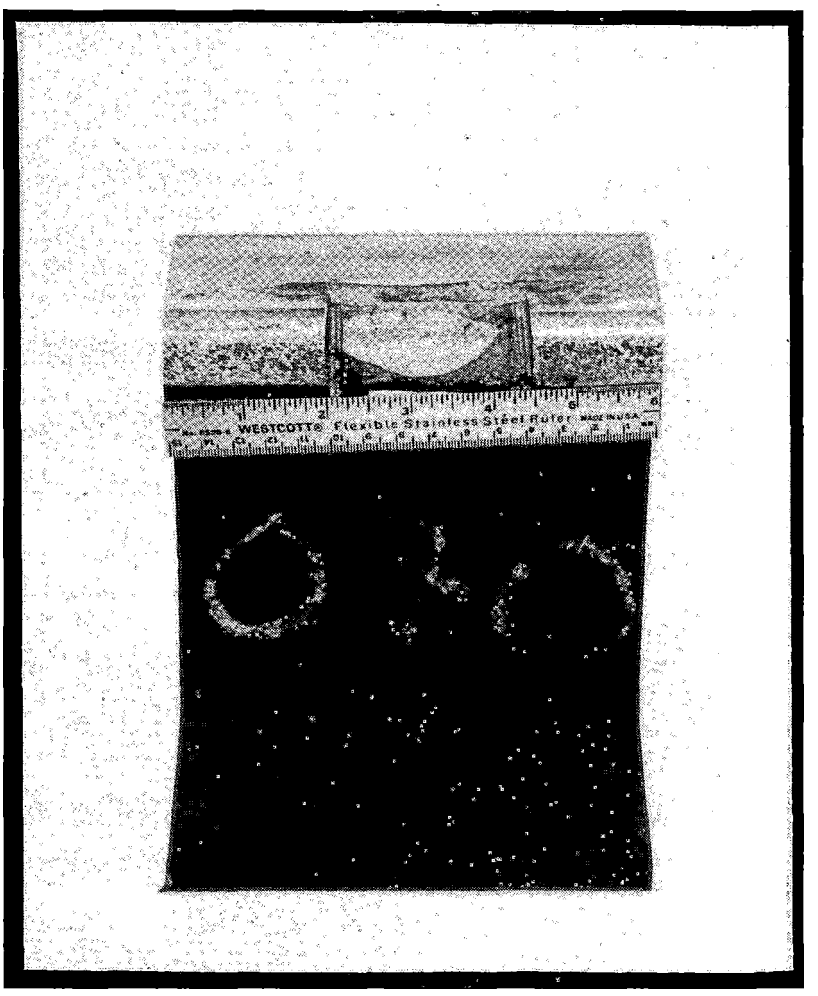

Figure 24. Bi-Planar Shell in Section 25B

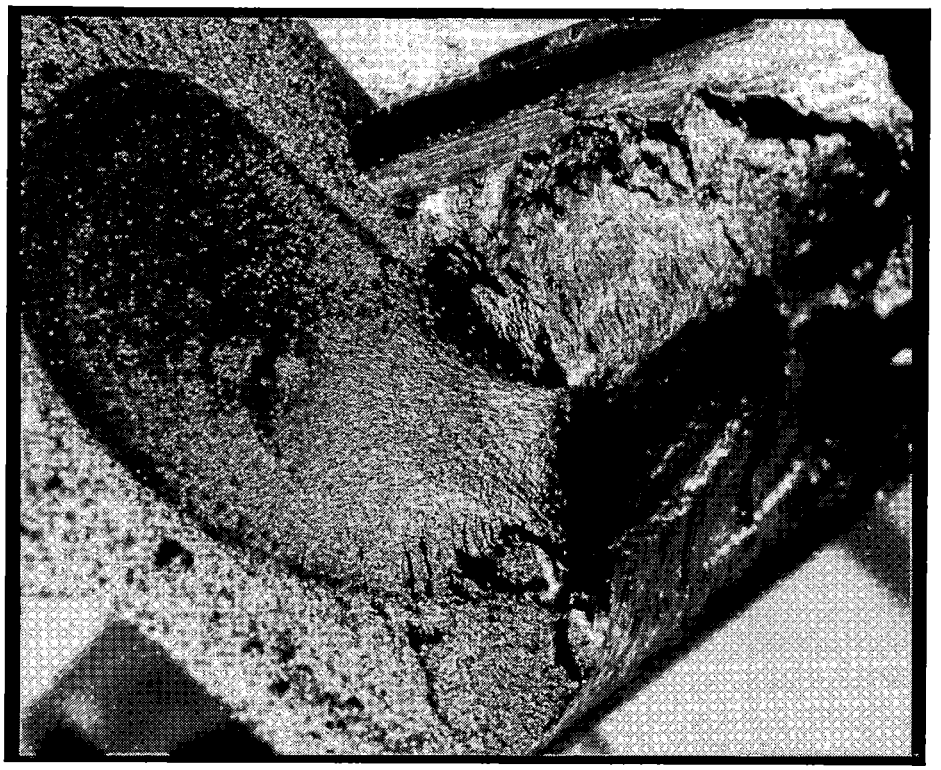

Figure 25. Detail Fracture from Bi-planar Shell

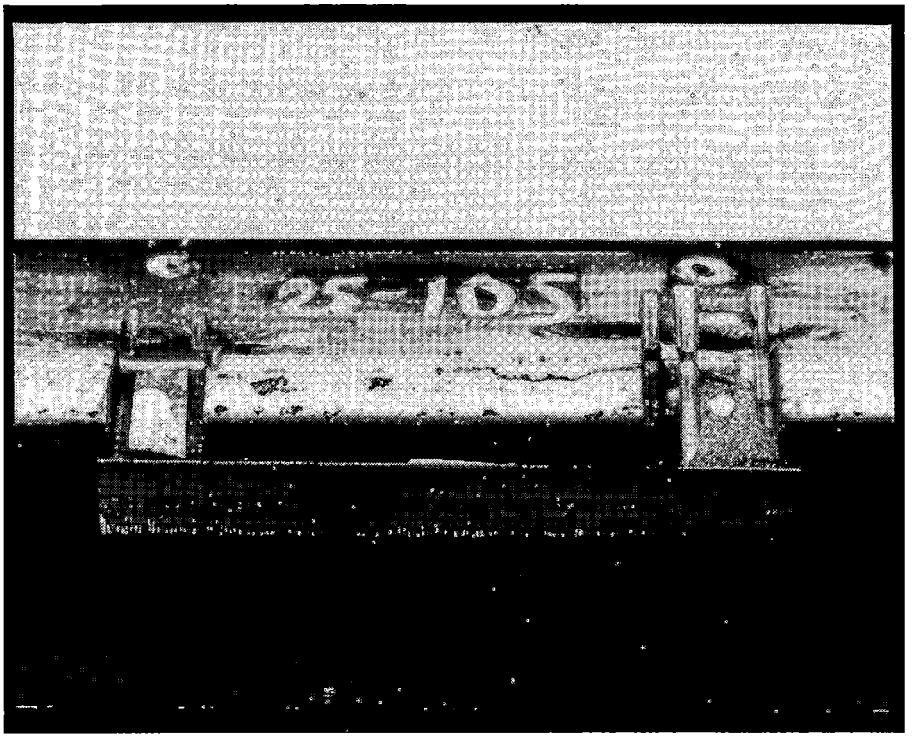

Figure 26. Very Small Shell Associated with Defect 25-0105

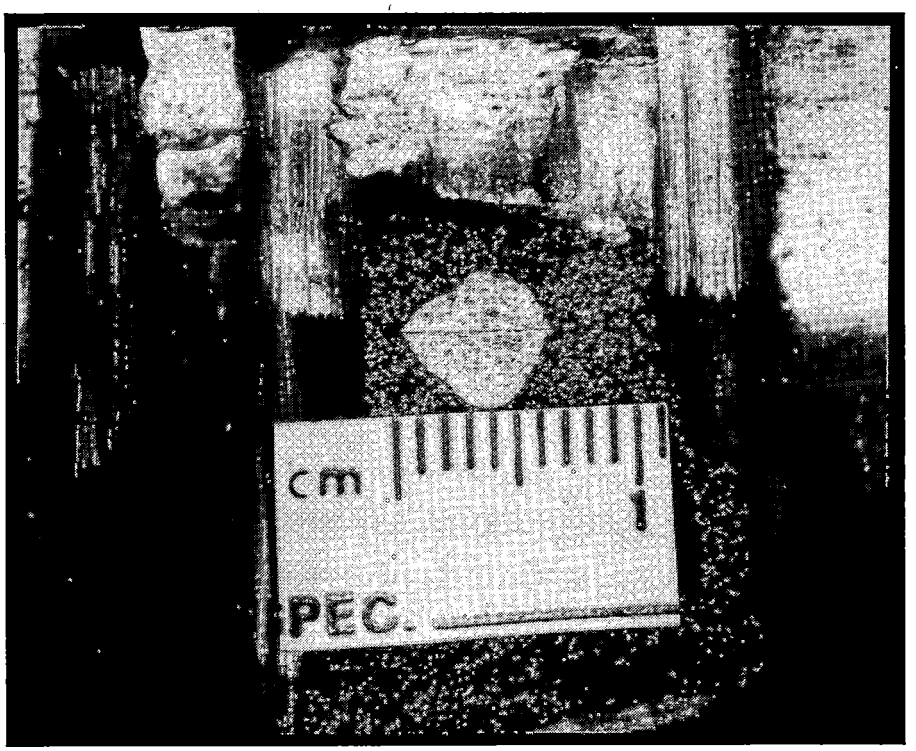

Figure 27. Close-up of Shell in Figure 26

The location of the initiation sites of 17 shells which formed DF's are given in Table 15. Figure 28 illustrates how the measurements were made with respect to the worn and new transverse profiles.

Table 15. Shell Initiation Locations

DEFECT	WORN PROFILE (IN.)		UNWORN PROFILE (IN.)	
	VERTICAL	HORIZONTAL	VERTICAL	HORIZONTAL
03-0658	0.55	0.62	0.64	0.64
03-0841	0.42	0.41	0.54	0.46
03-0857	0.46	0.48	0.54	0.51
25-0279	0.51	0.42	0.57	0.42
25-0292	0.39	0.33	0.46	0.33
25-0293	0.48	0.46	0.59	0.45
25-0307	0.37	0.35	0.43	0.37
25-0330	0.47	0.49	0.54	0.46
25-0499	0.48	0.40	0.52	0.41
25-0724	0.49	0.35	0.47	0.41
25-0890	0.26	0.28	0.35	0.39
25-1308	0.41	0.35	0.51	0.41
25-1352	0.24	0.16	0.30	0.25
25-1356	0.27	0.20	0.36	0.27
25-1359	0.25	0.16	0.34	0.23
25-1385	0.40	0.38	0.46	0.41
25-1654	0.50	0.57	0.55	0.63

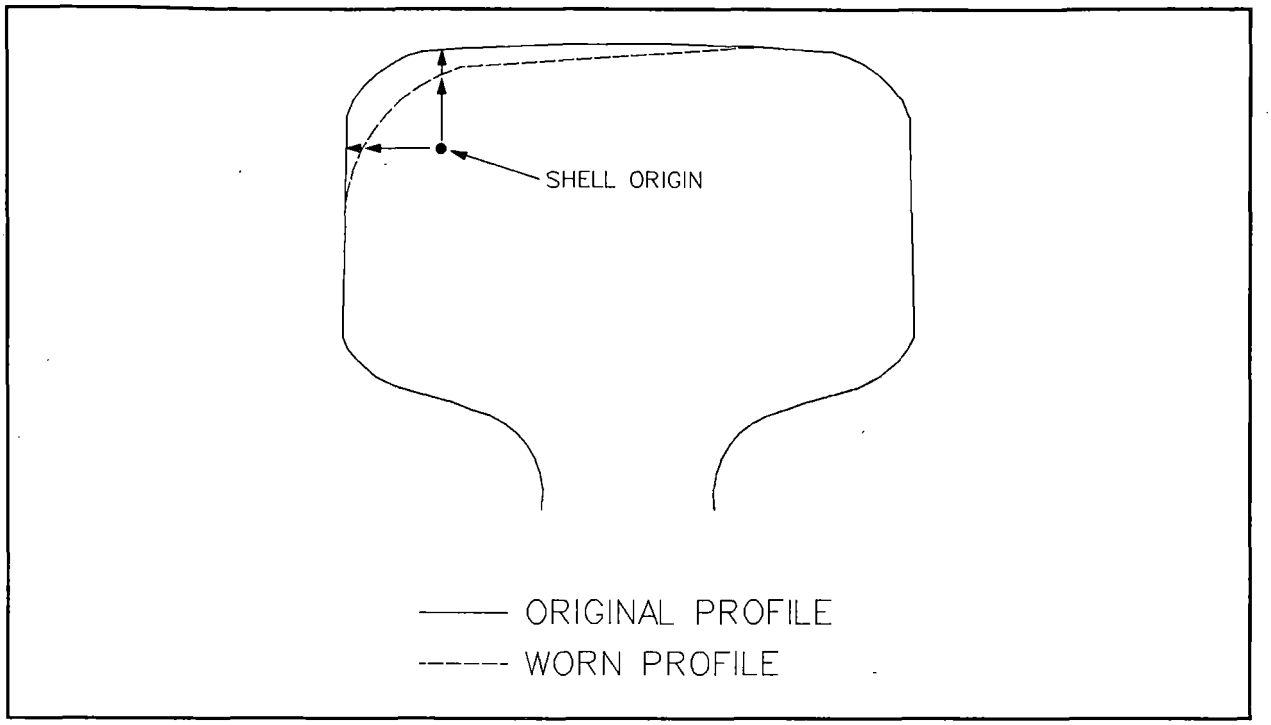

Figure 28. Vertical and Horizontal Locations of Shell Origin with Respect to Original and Worn Transverse Rail Profile

The shells formed 0.30-0.64 inches (7.6-16.3 mm) below the original rail surface and 0.23-0.64 inches (5.8-16.3 mm) in from the gage face. The corresponding values for the as-worn profile are 0.24-0.55 inches and 0.16-0.62 inches. Assuming a normal distribution, the initial location with respect to the unworn profile is given by a mean $\pm$ two standard deviations of 0.48 $\pm$0.19 inches (12.2 $\pm$4.8 mm) below the surface and 0.41 $\pm$0.21 (10.4 $\pm$5.3 mm) in from the gage face.

4.8 CRACK GROWTH STUDY

An example of the marker rings on the face of a detail fracture, 25-1308, is seen in Figure 29. The schematic in Figure 30, shows how the area of a DF was determined, following Orringer et al.[5] To calculate the crack size in terms of percentage of head area, the crack face area was divided by 4.86 for a 136-pound rail and 4.42 for a 132-pound rail. Crack growth data for the 12 defects are presented in Table 16.

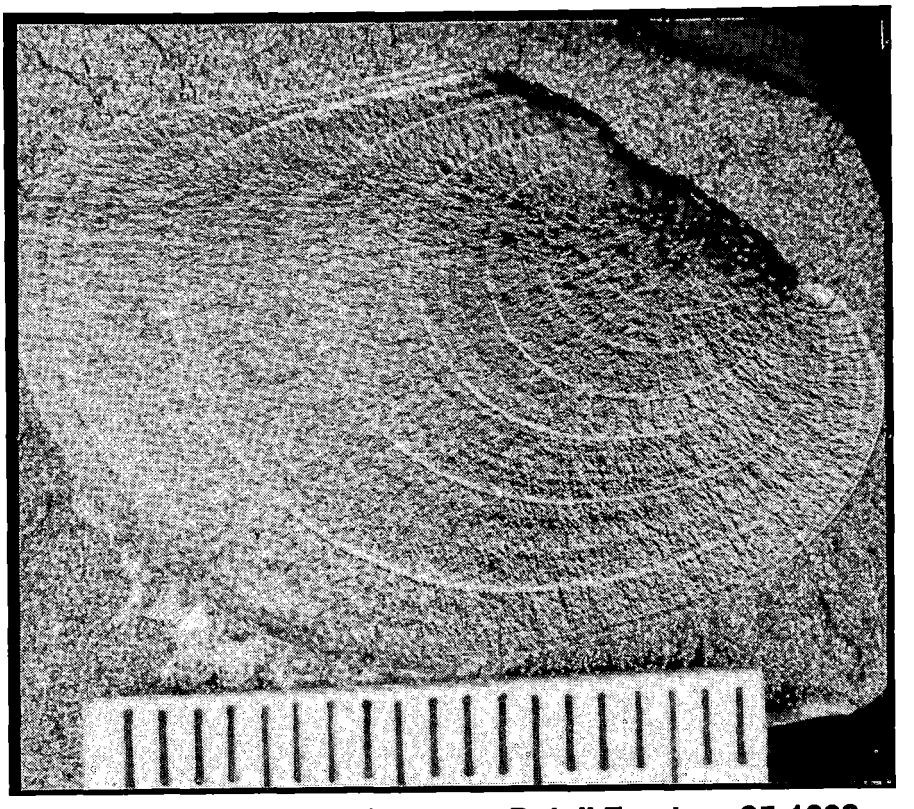

Figure 29. Marker Rings on Detail Fracture 25-1308

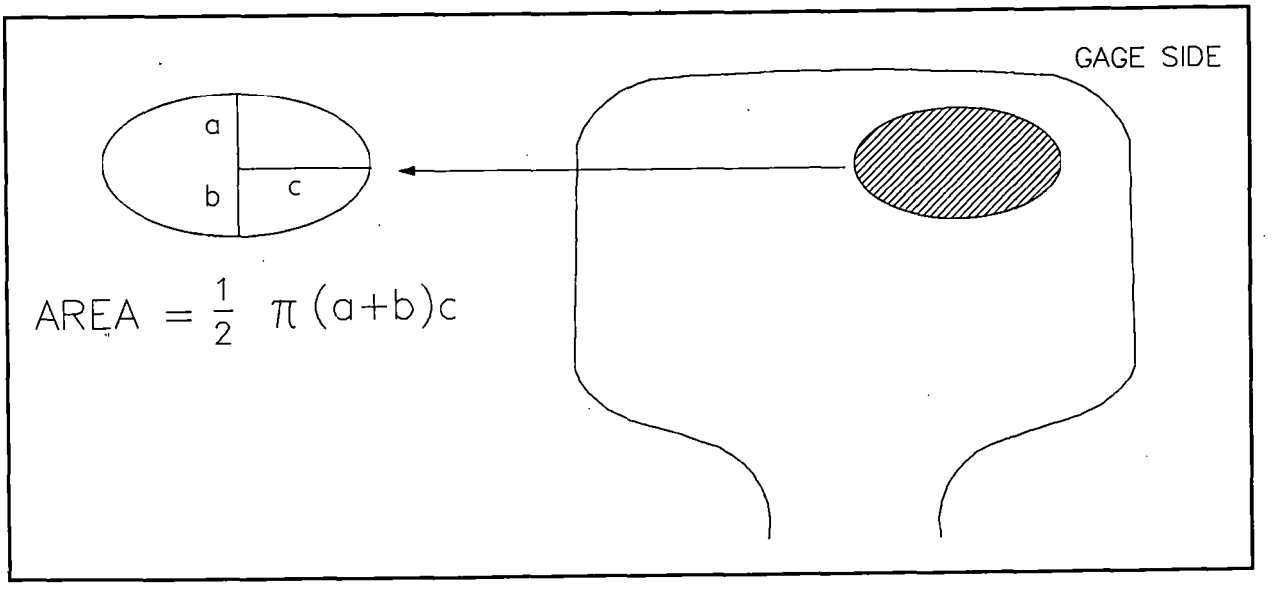

Figure 30. Calculation of Approximate Detail Fracture Size

Table 16. Detail Fracture Growth Data

MGT	a+b (in.)	2c (in.)	AREA SQ. IN.	% HEAD AREA
03-0539				
120.8	0.44	0.43	0.149	3.362
124.1	0.71	0.63	0.351	7.948
127.2	0.89	0.87	0.608	13.759
130	1.02	1.12	0.897	20.300
133.4	1.14	1.41	1.262	28.562
03-0541				
136.2	0.17	0.16	0.021	0.483
139.3	0.28	0.29	0.064	1.443
143	0.55	0.55	0.238	5.375
145.8	0.74	0.83	0.482	10.914
150.2	1.04	1.24	1.013	22.915
03-0576				
124.1	0.19	0.15	0.022	0.506
127.2	0.22	0.18	0.031	0.704
130	0.24	0.2	0.038	0.853
133.4	0.28	0.24	0.053	1.194
136.2	0.3	0.32	0.075	1.706
139.3	0.37	0.44	0.128	2.893
143	0.63	0.72	0.356	8.060
145.8	0.84	1.02	0.673	15.225
150.2	1.07	1.5	1.261	28.520

Table 16. Detail Fracture Growth Data -- (Continued)

MGT	a+b (in.)	2c (in.)	AREA SQ. IN.	% HEAD AREA
03-0592				
127.2	0.14	0.09	0.010	0.224
130	0.19	0.12	0.018	0.405
133.4	0.28	0.2	0.044	0.995
136.2	0.37	0.3	0.087	1.972
139.3	0.48	0.45	0.170	3.838
143	0.73	0.71	0.407	9.210
145.8	0.88	0.94	0.650	14.699
150.2	1	1.28	1.005	22.745
25-0279				
120.8	0.17	0.07	0.009	0.192
124.1	0.25	0.12	0.024	0.485
127.2	0.32	0.18	0.045	0.931
130	0.41	0.27	0.087	1.789
133.4	0.49	0.39	0.150	3.088
136.2	0.63	0.55	0.272	5.600
139.3	0.79	0.77	0.478	9.830
141.8	0.95	1	0.746	15.352
25-0322				
124.1	0.13	0.08	0.008	0.168
127.2	0.15	0.11	0.013	0.267
130	0.26	0.19	0.039	0.798
133.4	0.35	0.31	0.085	1.753
136.2	0.49	0.45	0.173	3.563
139.3	0.71	0.66	0.368	7.573

Table 16. Detail Fracture Growth Data -- (Continued)

MGT	a+b (in.)	2c (in.)	AREA SQ. IN.	% HEAD AREA
143	0.98	0.95	0.731	15.045
145.8	1.1	1.13	0.976	20.087
150.2	1.22	1.41	1.351	27.799
25-0330				
120.8	0.44	0.3	0.104	2.133
124.1	0.62	0.42	0.205	4.208
127.2	0.76	0.56	0.334	6.878
130	0.86	0.72	0.486	10.007
25-1308				
120.8	0.33	0.24	0.062	1.280
124.1	0.39	0.32	0.098	2.017
127.2	0.45	0.44	0.156	3.200
130	0.62	0.58	0.282	5.811
133.4	0.82	0.8	0.515	10.601
136.2	1.04	1.06	0.866	17.815
139.3	1.18	1.34	1.242	25.553
25-1316				
127.2	0.16	0.06	0.008	0.155
130	0.22	0.11	0.019	0.391
133.4	0.3	0.2	0.047	0.970
136.2	0.4	0.34	0.107	2.198
139.3	0.6	0.53	0.250	5.139
143	0.88	0.81	0.560	11.519
145.8	1.02	1.05	0.841	17.308
150.2	1.2	1.24	1.169	24.047

Table 16. Detail Fracture Growth Data -- (Continued)

MGT	a+b (in.)	2c (in.)	AREA SQ. IN.	% HEAD AREA
25-1356				
120.8	0.52	0.65	0.265	6.006
124.1	0.69	0.94	0.509	11.525
127.2	0.77	1.16	0.702	15.871
130	0.86	1.39	0.939	21.241
25-1359				
120.8	0.28	0.31	0.068	1.542
124.1	0.41	0.46	0.148	3.351
127.2	0.48	0.59	0.222	5.032
130	0.55	0.7	0.302	6.841
133.4	0.63	0.84	0.416	9.403
136.2	0.81	1.03	0.655	14.825
139.3	0.92	1.25	0.903	20.435
25-1372				
127.2	0.11	0.1	0.009	0.195
130	0.16	0.16	0.020	0.455
133.4	0.32	0.24	0.060	1.365
136.2	0.4	0.41	0.129	2.914
139.3	0.56	0.64	0.281	6.368
143	0.82	0.94	0.605	13.697
145.8	0.98	1.13	0.870	19.678
150.2	1.13	1.27	1.127	25.501

Growth as a function of MGT is plotted for one defect, 03-0576, in Figure 31. The shape of this plot was quite consistent for all the defects. Table 17 presents the parabolic regression data for each of the eight complete growth curves obtained.

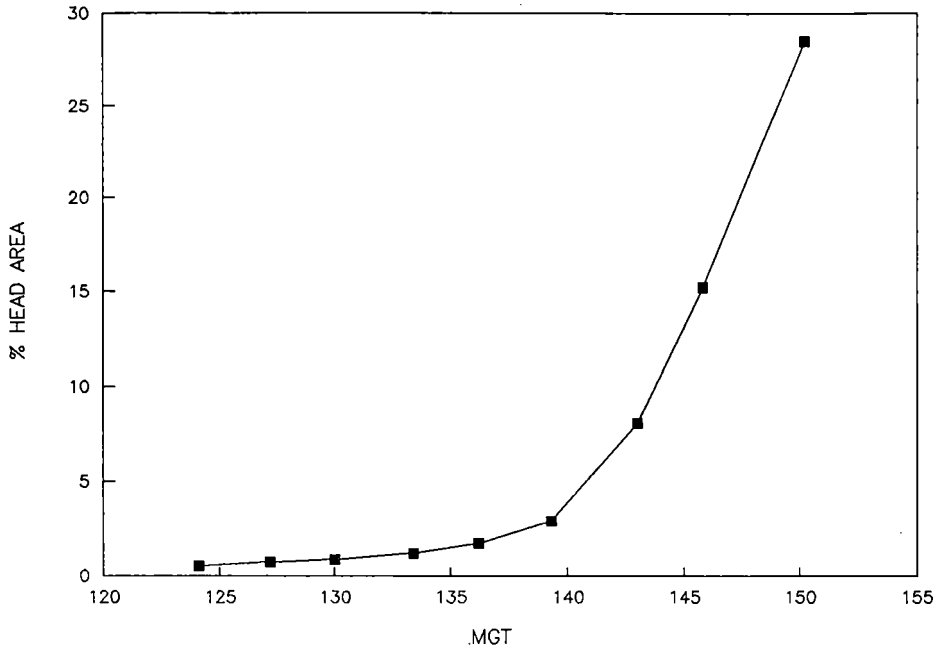

Figure 31. Crack Growth Versus Cumulative MGT for Detail Fracture 03-0576

Table 17. Regression Data for the Detail Fracture Growth Relation, %HA (>1%) = $A(MGT)^B$

RAIL	DEFECT	A	B	r
E 302	25-0279	0.15	1.65	0.985
A 284	25-0322	0.15	1.79	0.998
A 284	25-1308	0.04	2.11	0.991
A 284	25-1316	0.21	1.70	0.998
G 321	25-1372	0.19	1.70	0.999
L 294	03-0541	0.07	2.25	0.999
L 294	03-0576	0.02	2.44	0.988
L 294	03-0592	0.14	1.78	0.996

5.0 ANALYSIS

5.1 POSITION IN CURVE EFFECTS

The experimental results have been carefully scrutinized to reveal any undesirable influences. An effect of Position in Curve on the data has been virtually ruled out from the head height loss and track geometry measurements in the Results section.

The total number of rails in a single segment, was very small and this remains a potential problem in the analysis of the results. Under these circumstances the reproducibility of results becomes a significant factor and this has never been established at FAST. Furthermore, only the bare minimum of work to characterize the rail steels used in the experiment has been undertaken. These factors have to be kept in mind when attempting to draw hard conclusions from the data.

5.2 DETAIL FRACTURE DEFECT RATES

Table 12 shows that if the L 294 rails are excluded, Sections 03 and 25B exhibited about half the number of DF's experienced by Sections 25A and 25C. Figures 32 a-e reveal that, although Sections 03 and 25B produced DF's at lower MGT's than Sections 25A and 25C, and had similar initial defect rates, the final steady state defect rates were lower.

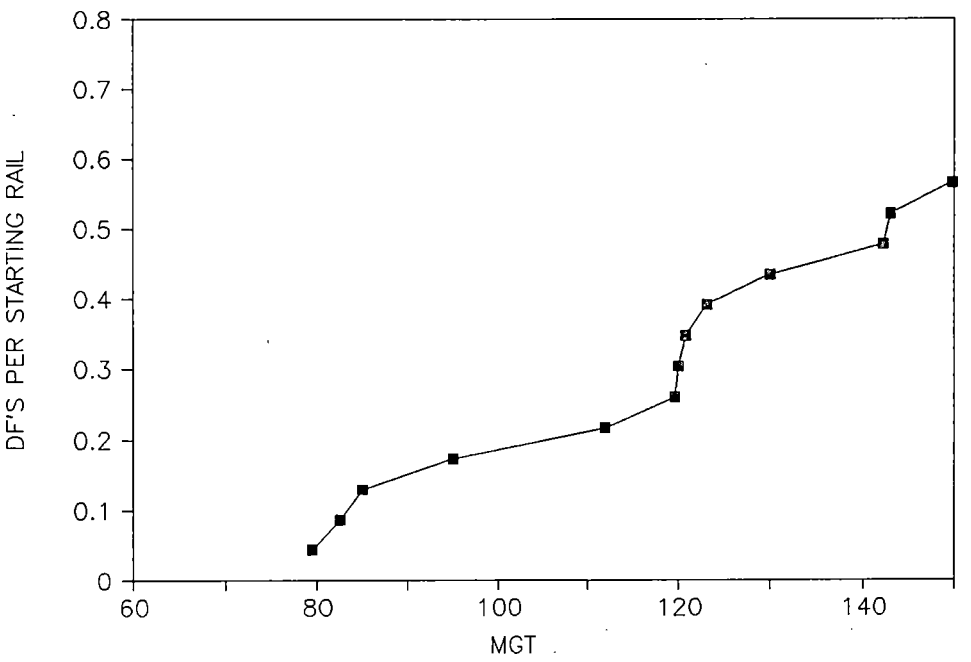

Figure 32(a). Detail Fractures versus MGT for Section 25A

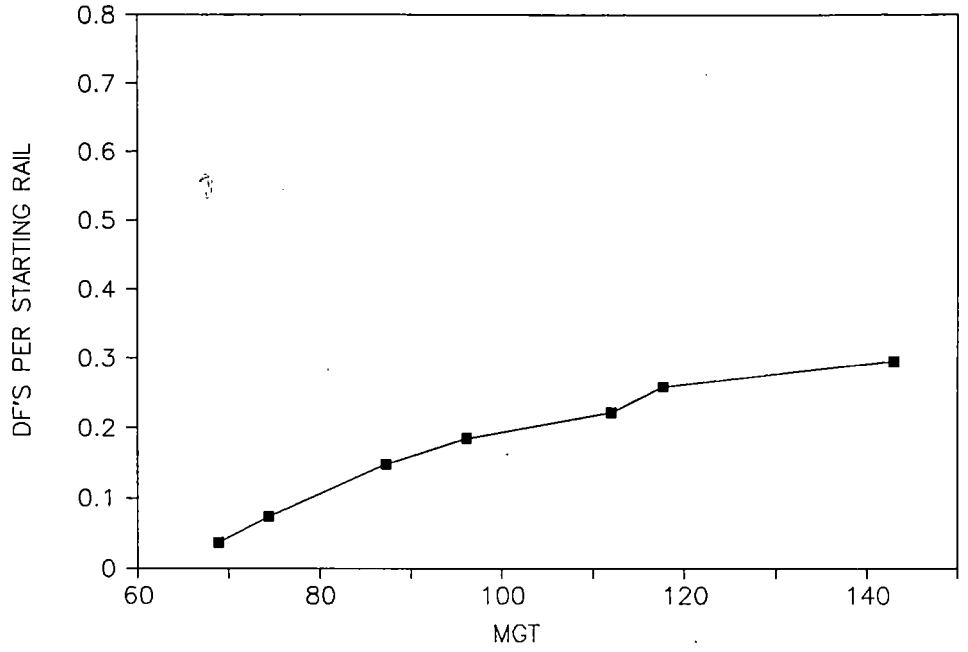

Figure 32(b). Detail Fractures versus MGT for Section 25B

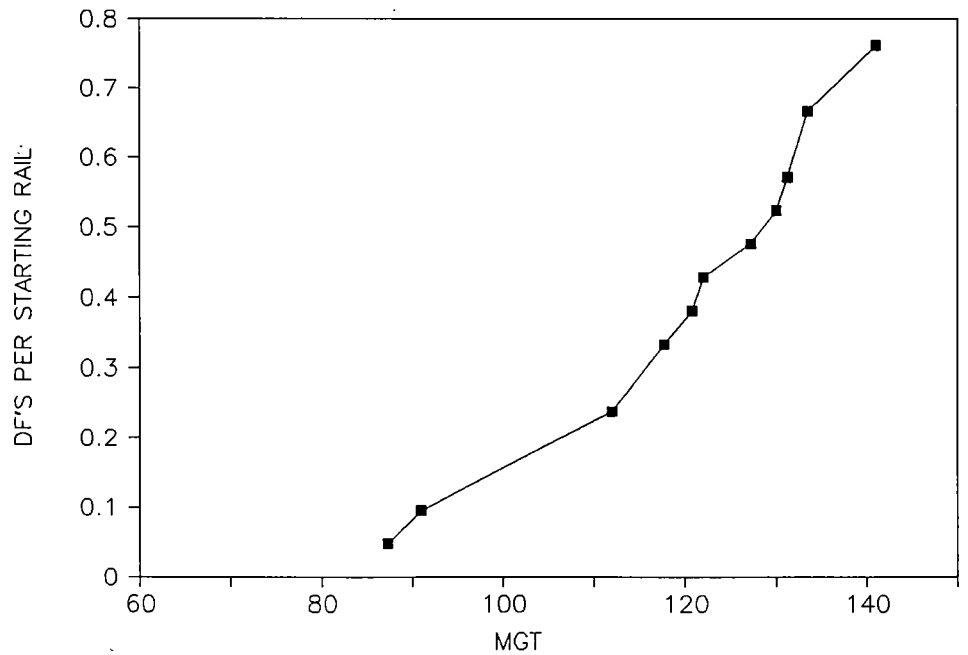

Figure 32(c). Detail Fractures versus MGT for Section 25C

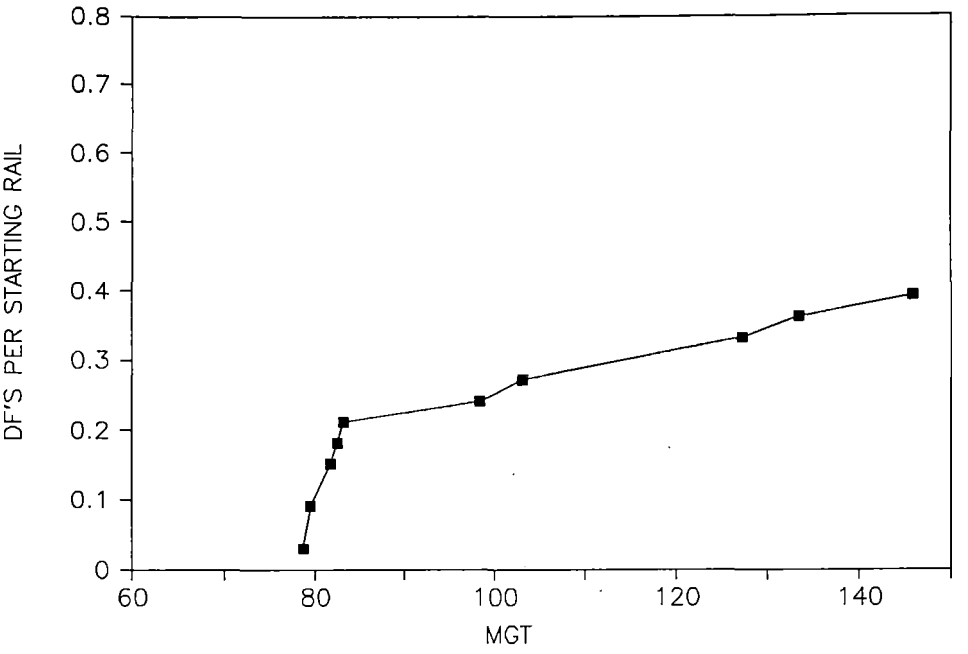

Figure 32(d). Detail Fractures versus MGT for Section 03

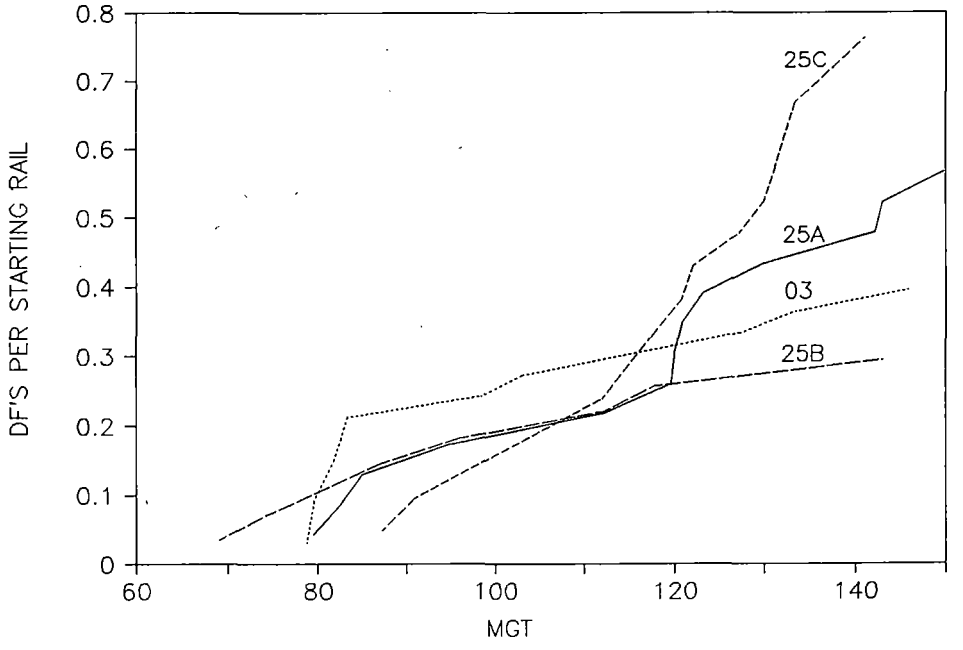

Figure 32(e). Detail Fractures versus MGT for All Segments

The DF defect rates presented in Figure 32 are based on the number of rails in track at the start of the tests. A number of rails, especially the B 285, were removed before the end of the experiment and thus the actual instantaneous defect rates would have been higher, particularly in Section 25B which contained a higher proportion of B 285 rails.

Table 18 takes into account rail removal and presents a slightly different picture of the DF rate in the various segments. The defect rates are based on five 30 MGT intervals. The rail population is given in feet of rail in track at the start of the interval. Even when the higher rail removal rate from Section 25B is considered, it is apparent that the defect rate pattern with MGT is different to those for the other two segments in Section 25. The similarity between Sections 25B and 03, noted above, is confirmed in that they exhibit a trend of declining defect rates with increasing MGT.

Table 19 provides the same type of information for each individual rail metallurgy. Despite the early removal of a number of rails, B 285 still had a sizeable population at 121 MGT. The DF rate for B 285 and D 296 steels was very low in the final 30 MGT period whereas for the A 284, G 321, E 302, and the L 294 steels the rates were accelerating. The A 284 and the G 321 rails stand out as having very high DF rates and the C 290, despite being one of the softest rails used, did not experience any defects.

Table 18. Actual Detail Fracture Defect Rates

MGT	POPULATION IN FEET OF RAIL	DF'S	DF'S PER FOOT X10^3	DF'S PER MILE
		SECTION 25A		
0-30	897	0	0.00	0
31-60	897	0	0.00	0
61-90	858	3	3.50	18
91-120	819	4	4.88	26
121-150	643	6	9.33	49
		SECTION 25B		
0-30	1053	0	0.00	0
31-60	1053	0	0.00	0
61-90	1053	4	3.80	20
91-120	733	3	4.09	22
121-150	733	1	1.36	7
		SECTION 25C		
0-30	780	0	0.00	0
31-60	780	0	0.00	0
61-90	780	1	1.28	7
91-120	780	6	7.69	41
121-150	780	9	11.50	61
		SECTION 03		
0-30	936	0	0.00	0
31-60	936	0	0.00	0
61-90	936	4	4.27	23
91-120	804	2	2.49	13
121-150	804	1	1.24	7

Table 19. Actual Detail Fracture Defect Rates for Individual Rail Metallurgies

MGT	POPULATION IN FEET OF RAIL	DF'S	DF'S PER FOOT X10^3	DF'S PER MILE
B 285				
0-30	858	0	0.00	0
31-60	858	0	0.00	0
61-90	819	5	6.11	32
91-120	297	2	6.73	36
121-150	297	1	3.37	18
A 284				
0-30	312	0	0.00	0
31-60	312	0	0.00	0
61-90	312	5	16.00	85
91-120	273	4	14.60	77
121-150	273	10	36.60	193
G 321				
0-30	312	0	0.00	0
31-60	312	0	0.00	0
61-90	312	2	6.41	34
91-120	312	5	16.00	85
121-150	253	5	19.76	104
D 296				
0-30	312	0	0.00	0
31-60	312	0	0.00	0
61-90	312	2	6.41	34
91-120	312	3	9.62	51
121-150	312	0	0.00	0
E 302				
0-30	351	0	0.00	0
31-60	351	0	0.00	0
61-90	351	0	0.00	0
91-120	351	0	0.00	0
121-150	351	2	5.70	30
L 294				
0-30	351	0	0.00	0
31-60	351	0	0.00	0
61-90	351	1	2.85	15
91-120	351	1	2.85	15
121-150	351	5	14.25	75

5.3 THE EFFECT OF THE DEGREE OF LUBRICATION ON FATIGUE.

If the K 290 rails are omitted, the distribution of rail types was exactly the same in Sections 25A and 25C, and it is possible to compare the overall results of the two segments directly. From Tables 5 a and c, if 150 MGT is taken as a maximum, the average life of the starting rails in Section 25A was 130.4 MGT compared with 143.4 in Section 25C. It seems unlikely that this 10 percent difference is a particularly significant one as the criteria for rail removal involved subjective judgment with respect to safety concerns.

Consider only the performance of B 285 in these two segments. The B 285 rails were removed from Section 25C after 132 MGT and after only 60-100 MGT in Section 25A. If this suggests a detrimental effect of higher lubrication, it is balanced by the fact that in Section 03 three B285 rails were removed by 87 MGT.

The defect results from Sections 25A and 25C are summarized in Table 20 on the basis of the number of starting rails. All rail steels that were not represented in both segments have been excluded while the number of shells includes those that produced DF's. The two sets of data are very similar. Furthermore, the distributions of DF's with respect to cumulative MGT (Figure 32e) were similar for the two segments although the actual defect rate was higher in Section 25C (Table 18).

Table 20. Comparison of Fatigue in Section 25A and Section 25C

SECTION	NO. RAILS	DF'S PER RAIL	SHELLS PER RAIL
25A	21	0.62	3.14
25C	21	0.76	3.09

Taking all the evidence into account, it is necessary to conclude that increasing the degree of lubrication from that provided in Section 25C to that seen in Section 25A had no effect on the rate of fatigue damage in the 6-degree curve. This does not of course mean that lubrication has no affect at all because in the nonlubricated curve in Section 07 there were no fatigue defects.[15]

5.4 THE EFFECT OF GAGE CORNER GRINDING ON FATIGUE

An initial reaction to the data given in Table 10 is that the grinding in Section 25B resulted in more fatigue than in the unground segments. The numbers are dominated, however, by the behavior of the B 285 steel which had a far higher shell rate in Section 25B than in either of the other two segments. This was not the case for any of the other rail metallurgies which exhibited shells. If all the rails are taken into account, the number of shells per starting rail is 2.3 in Section 25A, 5.9 in Section 25B and 2.3 in Section 25C. Excluding the B 285 rails gives 0.7, 0.9 and 2.0 respectively.

Table 21 presents the shell behavior of each B 285 rail. The shell rate varies even more between rails in a given segment than it does between different segments. For example, the rail with the highest rate in Section 25B, 0.60 shells per MGT, was located only one rail length away from the rail with the lowest rate of 0.03. These two rails were from the same heat.

Table 21. Shell Record for Individual B 285 Rails

LOCATION	HEAT NUMBER	NO. SHELLS PER RAIL	TOTAL LENGTH	MGT REMOVAL	SHELLS PER MGT
Sec25A					
0091-0115	1	12	90.5	59.6	0.20
0115-0139	1	5	18.0	79.5	0.06
0139-0160	1	10	36.8	100.0	0.10
0160-0173	2	1	7.0	100.0	0.01
0173-0196	2	15	44.8	100.0	0.15
Sec25B					
0679-0702	1	14	50.5	96.1	0.15
0702-0726	1	10	37.8	96.1	0.10
0726-0750	1	3	16.0	96.1	0.03
0750-0774	3	25	39.0	96.1	0.26
0774-0798	1	57	108.0	96.1	0.60
0798-0822	1	20	33.3	96.1	0.21
0822-0846	1	12	21.8	96.1	0.12
Sec25C					
1562-1583	4	2	12.8	132.0	0.02
1583-1608	3	6	36.3	132.0	0.05
1608-1632	1	10	28.3	132.0	0.08
1632-1656	3	4	7.3	132.0	0.03
1656-1668		4	14.0	132.0	0.03
Sec03					
0702-0726	5	2	13.0	87.0	0.02
0726-0750	5	3	19.0	87.0	0.03
0750-0774	5	1	0.3	150.0	0.01
0774-0797	3	2	1.3	150.0	0.01
0797-0820	3	10	47.5	66.0	0.15

It is possible, therefore, that a strong variability in the performance of the B 285 (heat No. 1) rails gives a distorted picture in Table 10. It can be stated quite categorically, however, that there is no evidence that the grinding was beneficial for shell prevention as had been hypothesized at the planning stage of the experiments.

5.5 EFFECT OF TRACK CURVATURE ON FATIGUE DEFECTS

Assuming all other things to be equal, a lower defect rate would be expected for Section 03 than Section 25 since the former is a 5-degree curve while Section 25 is a 6-degree curve. In Table 22 the occurrence of shells and DF's are compared for the two curves. The data show the effect of including and excluding the B 285 rails. Rails which were not replicated throughout the curves have been excluded.

Table 22. Comparison of Fatigue Defects in Section 25 and Section 03

SECTION	NO. RAILS	NO. SHELLS	NO. DFS	SHELLS/RAIL	DF'S/RAIL
Without B 285:					
03 (5°)	17	12	5	0.71	0.29
25 (6°)	48	52	33	1.08	0.69
With B 285:					
03 (5°)	22	30	7	1.36	0.32
25 (6°)	65	262	37	4.03	0.57

There is a much higher defect rate in Section 25 than in Section 03 with or without the B285 rails. While this fits the expected trend the degree of difference is surprising and raises the question as to whether the differences are due solely to curvature alone.

5.6 THE EFFECT OF RAIL METALLURGY AND INCLUSIONS ON FATIGUE

Perhaps the simplest perception of the influence of rail metallurgy on fatigue resistance is that the harder the steel the better. Even a cursory look at the results of the experiment shows that this is at best an oversimplification. Nonetheless, when the fatigue data are plotted as a function of the MGT carried by each individual metallurgy (Figures 33 and 34) there is an influence of hardness on fatigue performance.

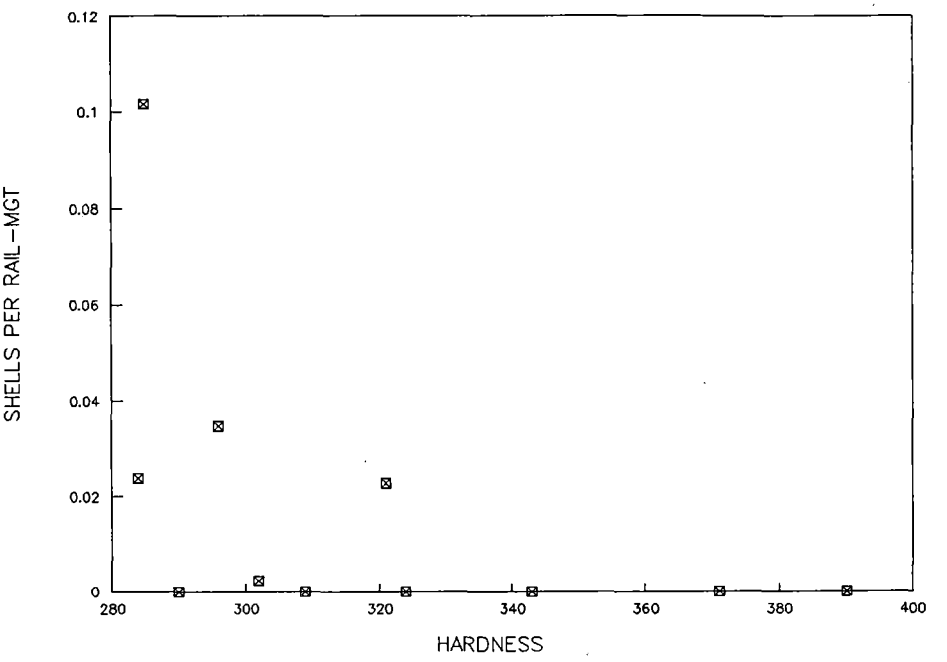

Figure 33. Effect of Rail Hardness on Shell Defect Rate

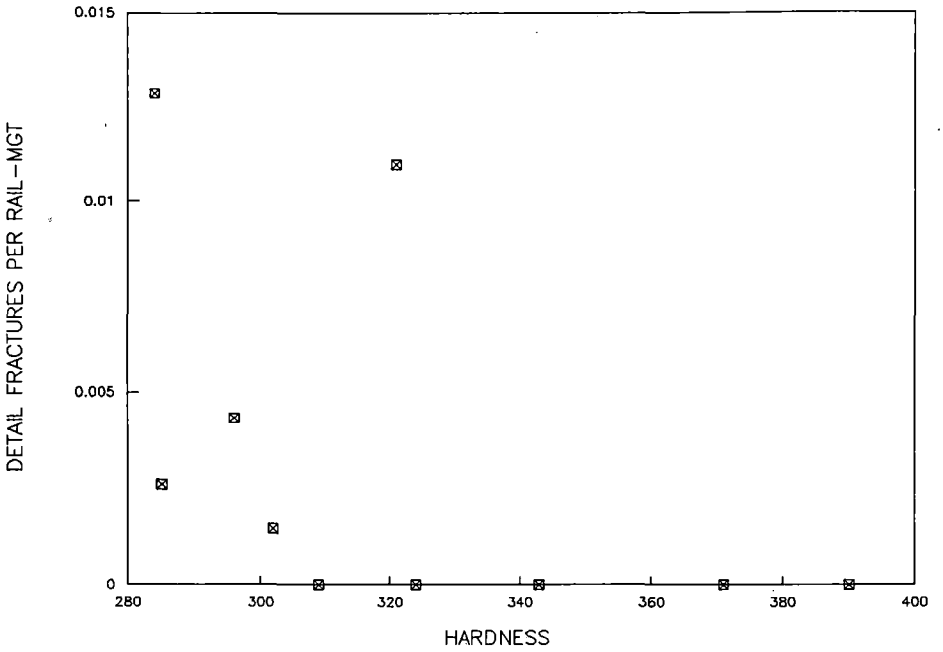

Figure 34. Effect of Hardness on Detail Fracture Rate

The parameter "defects per rail-MGT" has been used as a means of normalizing rail usage. Ten rails, of a given metallurgy, with each lasting the full 150 MGT represents 1500 rail-MGT for that metallurgy.

If the shell defect rate is correlated with inclusion parameters there is a discernible effect but, as with hardness, it is not an overwhelming one.

In specific cases there are clear indications that fatigue is controlled by both hardness and inclusions:

a) The A 284 and the J 371 steels were both from the same heat with the latter being head hardened to a higher hardness. The chemistries and inclusion contents should, however, be identical. The A 284 steel experienced a moderately high defect rate whereas the J 371 exhibited only a single shell.

b) The three softest steels were separated by a mere six points on the Brinell hardness scale yet produced a very wide range of defects.

c) The B 285 rail steel gave a very high shell defect rate yet the volume fraction of oxides was slightly lower than that of the D 296 which had a much lower shell defect rate. The oxide stringer numbers for the two steels were very different, however, being greater for the B 285 rail steel.

d) The F 309 rail steel, which did not produce any defects, contains more oxides than the G 321 steel, which had a moderately high defect rate. The distribution of those oxides was obviously different though, as seen in the much lower stringer number for F 309.

e) The C 290 steel, which did not exhibit any defects, had an oxide stringer number higher than the A 284 rail, which did have a number of defects. The former, however, contains a factor of 10 lower volume fraction of oxides.

Examples such as these indicate that the rail hardness, volume fraction of oxides and the nature of the dispersion of oxides all contribute to the probability of shell formation. This reasoning led to the formulation of a complex parameter, the Shell Index (SI), incorporating inclusion and hardness terms.

$$SI = Ln \left[\frac{\%\text{OXIDE VOLUME FRACTION} \times \text{OXIDE STRINGER LENGTH}}{\text{HARDNESS}^2} \right]$$

Figure 35 shows that SI separates those steels which did exhibit shells from those which did not. Also there is a reasonably good linear relation between shell rate and SI for the defect producing steels. The shell defect rate is based on the total number of shells including those which initiated DF's.

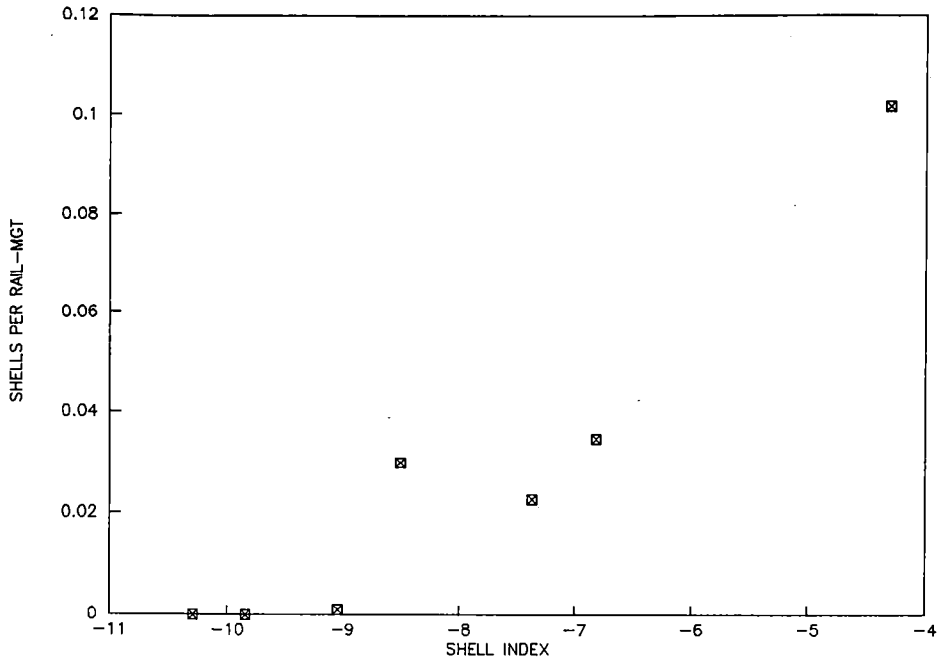

Figure 35. Shell Defect Rate as a Function of the Shell Index

Although the accumulation of more data may show that the SI parameter chosen here has not been optimized, it does provide useful insights into the effect of microstructural parameters on fatigue. Further investigation of this approach in developing rail steel specifications would, therefore, seem to be justified.

5.7 THE EFFECT OF WEAR RATE ON FATIGUE

The interest in this issue involves the possibility that an increase in wear rate could help reduce the incidence of fatigue damage in rails. The intention was to produce different gage face wear rates in Sections 25A and 25C to test this effect. Although lubrication levels were different in the two sections, the gage face and head height wear rates were not significantly affected. If there is some benefit to be gained from a higher wear rate, it does not, therefore, show up in this experiment.

The only variation in wear rates were associated with rail steel hardness. The harder the steel the lower both the wear rate and incidence of fatigue. Any positive influence of increasing hardness on fatigue resistance obviously outweighs any detrimental effect of lower wear rate on fatigue.

Two things remain to be tested, therefore, with regard to the influence of wear rate on fatigue failure rates. The first is the influence of wear rate for a given hardness of rail with lubrication the controlling influence. The second is the artificial control of "wear rate" by rail grinding.

5.8 DETAIL FRACTURE GROWTH RATES IN CURVED TRACK

The data presented in Table 17 show that the growth of the individual detail fractures, as a function of MGT, does not vary very much. This can be illustrated by superimposing all the growth plots (Figure 36). To normalize the data, a crack size of 1-percent head area has been taken as the starting point of growth at zero MGT.

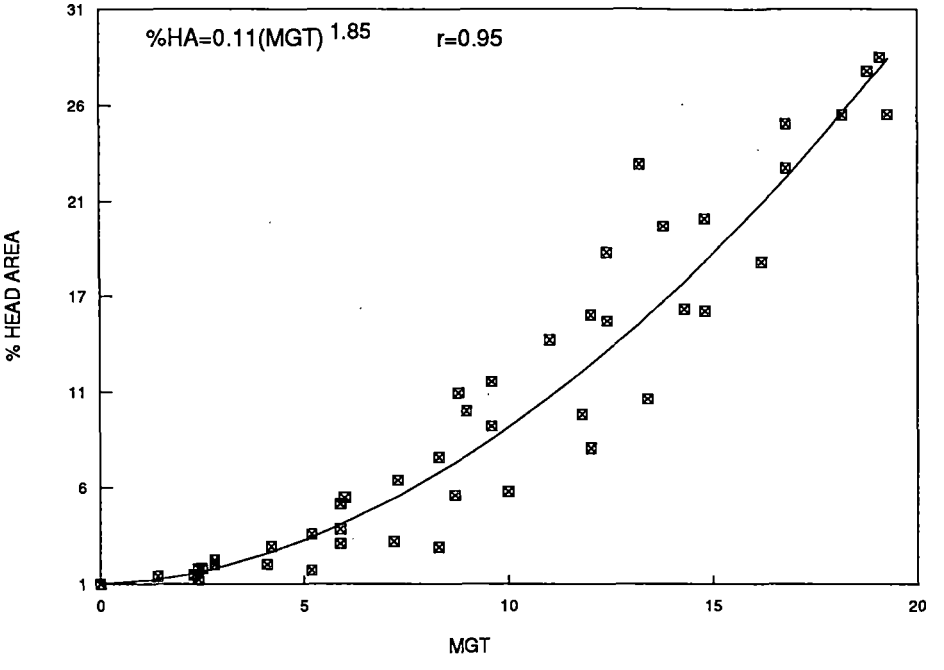

Figure 36. Normalized Crack Growth Based on all the Detail Fracture Data

The plot confirms the consistency of the data and also indicates that for growth beyond 10-percent head area the pattern of behavior could be well represented by a straight line. Table 23 presents the linear regression data for the nine defects which had sufficient data beyond the 10-percent head area size. The scatter in the slope values is not large with the average being very close to 2. If, on the other hand, the composite data in Figure 36 for sizes greater than 10-percent are regressed, the slope is 1.6.

Table 23. Regression Data for the Detail Fracture Growth Relation, %HA (>10%) = C + m(MGT)

STEEL	DEFECT	C	m	r
A 284	25-0322	-7.6	1.88	0.999
A 284	25-1308	-23.3	2.53	0.999
A 284	25-1316	-4.6	1.72	0.996
G 321	25-1356	*	1.64	0.996
G 321	25-1359	-15.6	1.87	0.999
G 321	25-1372	-3.5	1.61	0.991
L 294	03-0539	*	2.39	0.999
L 294	03-0592	-8.7	1.88	0.999
L 294	03-0576	-27.1	1.88	0.999

*Insufficient data to determine the MGT at 1%HA

6.0 DISCUSSION

Each of the three previous FAST experiments has produced its own individual characteristics. The experiment reported here was no exception. The unusual features in this case being the extensive occurrence of high rail corrugation, for the first time, and an unprecedented number of shells. For the B 285 rail, there is strong evidence that these were linked.

The only major differences in experimental procedure with respect to previous experiments were (1) the train ran in a single direction for the first 120.8 MGT with very limited train reversal subsequently, (2) the newly constructed loop included a 6-degree curve, and (3) lubrication was solely restricted to the outer rail for the first 90 MGT with slight contamination of the inner rail between 90 and 150 MGT. It is not obvious why these operating differences should result in the rail behavior observed.

It is necessary to conclude that the difference in the amount of lubricant supplied to Sections 25A and 25C did not produce any discernible difference in fatigue behavior. Furthermore, the specific high rail gage corner grind used did not have any beneficial effect on fatigue resistance. This does not prove that, in general, there is no effect of grinding and lubrication on fatigue defect rates. It has simply been demonstrated that the specific experimental conditions employed were too limited in scope to determine any such effects.

The metallurgical data have resulted in the introduction of the Shell Index. The interactive influence of rail hardness, oxide volume fraction and the tendency for oxide stringer formation on shell initiation has thus been documented for the first time. This is a significant step forward in understanding the overall effects of metallurgy on rail performance. It could play a major role in the development of new rail steel specifications based on fatigue resistance. It also demonstrates that attempts to classify fatigue resistance of a rail steel on the basis of a single influence are likely to be misleading.

One test of the usefulness of the Shell Index could be obtained by determining its value for the two B 285 rails which produced such different shell defect rates in Section 25B. Although it is difficult to believe that the inclusion levels could be so different, since they were from the same cast, it is not beyond the realms of possibility with ingot rail.

One potentially controversial point about the Shell Index is that oxide inclusion data were determined from a single 20 x 10 mm sample of rail taken at random, in a longitudinal sense, at the depth where shells occur. If the progress made so far is to be satisfactorily consolidated, it will be necessary to be much more rigorous in future investigations by examining a number of samples from each steel.

It was not possible to determine the effect of wear rate on the rate of shell formation since both strongly correlated with hardness. The real test of the PHOENIX prediction that a moderate head height loss can help to reduce the incidence of shells and DF's will require an experiment in which head height loss is artificially controlled through rail head grinding.

In the comparison between the defect rate in Section 25 with that in Section 03, it is reassuring that the 6-degree curve provided the higher rate. However, the very large difference between them is unexpected and would require further confirmation before the cause could be attributed purely to curvature.

The experiment produced a lot of very useful information on the rate of DF growth with MGT in curved track. On average, the DF's grew at about 1.6 percent to 2-percent head area per MGT between 10 percent and the largest size of 28 percent. An approximately linear growth rate was also observed in the previous FASTKRAX experiment for defect sizes up to 60 percent.[5]

The overall picture emerging, then, is that the safe crack growth life of a DF, that is, between the detectable size of 10 percent and what might be considered a rejectable size of 60 percent could involve a simple linear growth pattern.

The growth rate was the same in the current experiment for both 5- and 6-degree curves and about the same as in the FASTKRAX experiment with tangent track. This aspect of the results will require more detailed analysis because the Volpe National Transportation Systems Center's DF growth model predicts that there should be a strong influence of track curvature on growth rate. Given the complex nature of the DF and the factors influencing its behavior, this will require a separate investigation.

One intriguing aspect of the fatigue results is that while the B 285 rails produced many shells they yielded few transverse defects. The DF:shell ratio for this steel was, therefore, very low (Table 24). The ratio for D 286 was four times greater while for all the other steels, which exhibited fatigue defects, it was more than 40 times higher. The DF:shell ratio declined with an increasing SI. This would suggest that the factors which encourage shell initiation discourage DF formation.

Table 24. Ratio of Detail Fractures to Shells

RAIL	DF'S	SHELLS	DF/SHELL RATIO
A 284	19	33	0.58
B 285	6	234	0.03
D 296	5	40	0.13
E 302	2	3	0.67
G 321	12	25	0.48
L 294	7	13	0.54

It is interesting to speculate that this observation might be connected to shell crack growth rate which in turn could be a function of SI. While the effect of strength on fatigue crack propagation, in general, has been inconclusively debated for years, it is certainly possible that a high oxide content, particularly in the form of near continuous stringers, would encourage shell crack growth.

The analytical work of Keer et al suggests that once a shell has grown beyond a certain size the probability of a DF forming decreases.[16] Shells which formed DF's ranged from 2 mm to 40 mm long when the DF was initiated, while those without transverse cracks were all longer than 40 mm. A high shell crack growth rate might, then, discourage the formation of transverse defects.

If the volume fraction of oxides and their distribution affect the growth rate of the shell, a steel with as many oxide stringers as the B 285 could then produce few DF's but many shells. In the case of the A 284 steel, on the other hand, it is possible to postulate that the oxide content was not high enough to generate a large number of shells but that the shell growth rate, without help from a suitable dispersion of oxides, was slow enough to result in a high probability of downward turning cracks.

Shell size and the formation of detail fractures has another interesting aspect in this experiment. DF's formed from shells only 2 mm long. Such occurrences in the field might lead to misinterpretation of defect type. This possibility provides the incentive for regular metallurgical analysis to ensure that the correct picture of rail defects is obtained. The experience with the suspected DF's, which turned out to be vertical upturning cracks emanating from a long shell, in the current experiment, serves to reinforce this point.

Putting the results into perspective, with respect to previous experiments, it is notable that in RME II, which involved continuous lubricated running, there were 14 head defects in the whole of Section 03 in 290 MGT. This compares with 15 DF's in only about one-third of Section 03 in 150 MGT of the current experiment; a defect rate of about six times that in RME II. It is reasonable to assume that, in general, the rails used in the current experiment were at least as defect resistant as those used in RME II.

It is not possible to compare the shell population on the same basis because shells were not recorded in RME II but undocumented evidence from researchers involved in the work indicate that there were far fewer shells than in the current experiment.

Why should the experiment be more severe in terms of fatigue damage than the RME II experiment? Two differences in operation can be offered as possibilities. In the previous FAST experiments both rails were well lubricated. This was not the case in the DOG experiment even after the introduction of contamination of the inner rail at 120.8 MGT. The differential between outer and inner rail lubrication prior to 90 MGT resulted in higher wheel rail spreading forces.

In RME II the train was reversed every few days (approx. 1 MGT intervals) whereas in the DOG experiment it was run in a single direction for most of the time. It is possible, but not substantiated, that this single direction running helped the formation of high rail corrugations not seen previously and that the corrugation encouraged the formation of shells. It is also possible that bi-directional running hinders the initiation of shells but encourages their growth in preference to forming transverse defects.

The high defect rate in the DOG experiment serves to highlight the very low defect rate in RME III. The employment of alternating periods of dry and lubricated running in the latter certainly seems to be the most likely explanation for the differences observed. It could be that this effect was simply one of wearing in a more conformal profile at the start of the trial. If so the grinding experiments being carried out in the new heavy axle load experiments in Section 25 could provide more supporting evidence for the benefits of the concept tried in RME III.

Certainly if one of the ultimate goals of the current work is to develop the most economical way of controlling hazardous defects then the results of RME III must not be forgotten. Further, the potential role of profile grinding new rail has to be given some prominence in the future.

In seeking pointers with which to guide future FAST experiments, there are a number of issues which can be raised. In particular it is essential to have some common rails to enable reliable comparisons to be made. This has, hopefully, been taken care of for the experiment with the 125-ton capacity cars by the use of some B 285 rails and the minimum number of two other rail steels which exhibited fatigue defects in the DOG experiment.

Since the occurrence of a shell constitutes a fatigue failure, these defects need to be monitored as carefully as DF's. To follow-up the development of the Shell Index, much better microstructural characterization of the rail steels is required. The determination of inclusion levels needs to include volume fraction of oxides as well as some measure of oxide stringer length and clustering tendency. More effort needs to be channeled into determining the origins of shells and DF's with respect to oxides, the nature of the oxides involved, and their size.

7.0 CONCLUSIONS

1. Shells originated at approximately 12 mm (0.5 inch) below the surface of the unworn rail and 20 mm (0.4 inch) in from the gage face. All shells examined had a central step feature which is associated with inclusions.

2. The occurrence of shells in the rail steels tested has been related to a Shell Index which incorporates oxide volume fraction, a measure of oxide stringers and hardness. The indications are that shell formation can be suppressed by increasing rail hardness, reducing the volume fraction of oxides, reducing the number of oxide stringers, or some combination of these actions.

3. The range of shell sizes that initiated detail fractures was 2 mm to 40 mm. None of the many shells longer than 40 mm resulted in a detail fracture.

4. The high incidence of shells in the B 285 rail was associated with high rail corrugations not seen previously at FAST.

5. The presence of corrugation and shells in the B 285 rails did not necessitate any track maintenance to restore track geometry.

6. The rate of detail fracture growth was very consistent for the defects measured in both 5- and 6-degree curves. The average growth from 1 percent to 28 percent head-area involved 19 MGT of traffic. Growth from 10 percent could be approximated by a linear relation in which the average growth rate was between 1.6 and 2 percent per MGT.

7. The variation in the degree of lubrication between that sustained in Section 25A and the lower level in Section 25C did not have any discernible effect on head height loss, gage face wear or fatigue.

8. The rate of fatigue defects was higher in the 6-degree curve than in the 5-degree curve for almost the same distribution of rail types.

9. The specific gage corner profile ground on the high rails in Section 25B did not reduce the fatigue rate with respect to the other two segments of Section 25.

REFERENCES

1. Reiff, R.P. "Rail/Wheel Lubrication Studies at FAST," *Lubrication Engineering*, 42, pp 340-349, 1986.

2. Dahlman, G. and M. Stehly. "Energy Savings from Rail Lubrication on the Santa Fe Railway," Second International Symposium on Wheel/Rail Lubrication, Memphis, 1987, Association of American Railroads.

3. Steele, R. K. and P. Clayton, unpublished FAST data.

4. Steele, R. K. and M. Joerms. "A Fatigue Analysis of Wheel Load on Rail Life," AAR Report R-689, September 1988.

5. Orringer, O., Y.H.Tang, J.E.Gordon, D.Y.Jeong, J.M.Morris and A.B.Perlman, "Crack Propagation Life of Detail Fractures in Rails," U.S. Dept. of Transportation Report DOT/FRA/ORD-88/13, October 1988.

6. Longson, B. H. and S.T.Lamson. "Development of Rail Profile Grinding at Hamersly Iron," Association of American Railroads, Second International Heavy Haul Railway Conference, Colorado Springs, September 1982.

7. Sonon, D. E., J. V. Pellegrino and J. M. Wandrisco. *A Metallurgical Examination of Control Cooled, Carbon-Steel Rails with Service Developed Defects, in Rail Steels -- Developments, Processing and Use*, D. H. Stone and G. G. Knupp, eds, ASTM STP 644, 1978, pp. 99-117

8. Marich, S., J. W. Cottam and P. Curcio. "Laboratory Investigation of Transverse Defects in Rails," First International Heavy Haul Railway Conference, Institute of Engineers of Australia, Perth 1978.

9. Skinner, D. H. and P. A. Judd. "A Metallographic Study of Fatigue Defects in Rails," 34th Australian Institute of Metallurgists Annual Conference, Queensland 1981.

10. Rice, R. C., R. Rungta and D. Broek. "Post-Service Rail Defect Analysis," Third Interim Report, U.S. Dept. of Transportation, July 1983.

11. Steele, R. K. and R. P. Reiff. "Rail: Its Behavior and Relationship to Total System Wear," Association of American Railroads, Second International Heavy Haul Railway Conference, Colorado Springs, September 1982.

12. Heiss, J., et al, Derailment at FAST, July 1, 1986, FRA Report FRA/ORD-88/01, January 1988.

13. Kish, A., G. Samavedam and D. Jeong. "The Neutral Temperature Variation of Continuous Welded Rails, AREA Bulletin 712 October 1987.

14. Sugino, K., H. Kageyama and H. W. Newell. "Detection Method for Harmful Inclusions in Rail Steel," AREA Bulletin 716, 89, 1988, pp. 230-259.

15. Reiff, Richard P. "Defect and Wear Studies on Premimu and Standard Rails, Rail Wear Experiment RME IV, 0-110 MGT," FAST/HTL Technical Note TTC-89-09, July 1989.

16. Keer, L., T. M. Farris and R. K. Steele. "On Some Aspects of Fatigue Crack Growth in Rails Induced by Wheel/Rail Contact Loadings," Second International Symposium on Contact Mechanics and Wear of Wheel Rail Systems, University of Rhode Island, 1986, University of Waterloo Press.

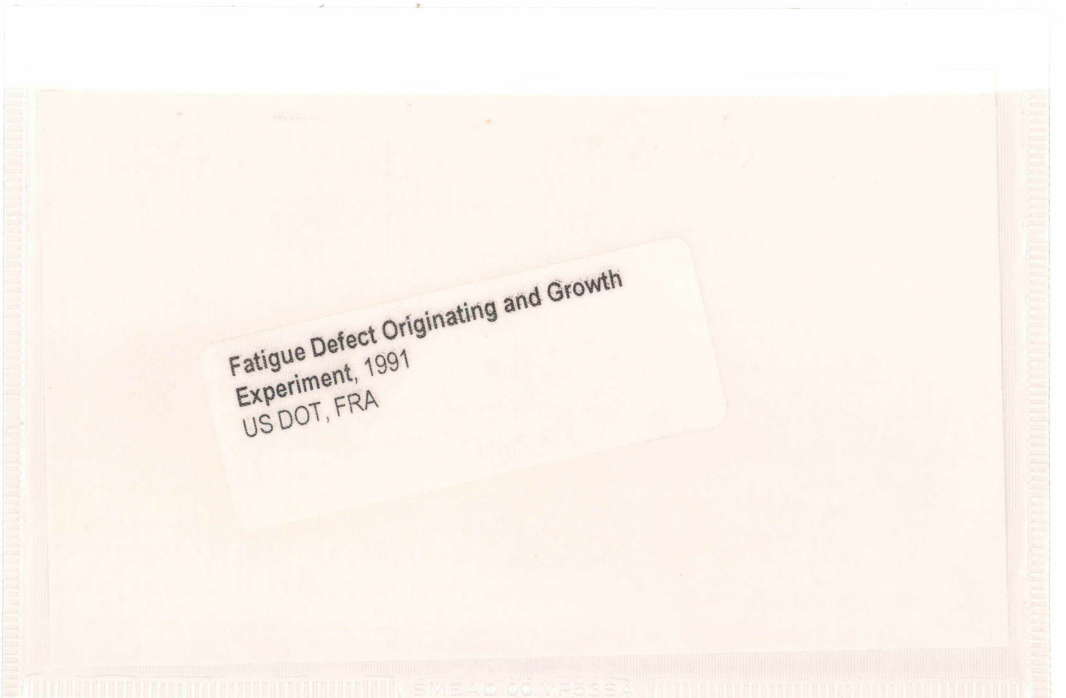

METRIC CONVERSION FACTORS

Approximate Conversions to Metric Measures

Symbol	When You Know	Multiply by	To Find	Symbol
		LENGTH		
in	inches	°2.5	centimeters	cm
ft	feet	30	centimeters	cm
yd	yards	0.9	meters	m
mi	miles	1.6	kilometers	km
		AREA		
in^2	square inches	6.5	square centimeters	cm^2
ft^2	square feet	0.09	square meters	m^2
yd^2	square yards	0.8	square meters	m^2
mi^2	square miles	2.6	square kilometers	km^2
	acres	0.4	hectares	ha
		MASS (weight)		
oz	ounces	28	grams	g
lb	pounds	0.45	kilograms	kg
	short tons (2000 lb)	0.9	tonnes	t
		VOLUME		
tsp	teaspoons	5	milliliters	ml
Tbsp	tablespoons	15	milliliters	ml
fl oz	fluid ounces	30	milliliters	ml
c	cups	0.24	liters	l
pt	pints	0.47	liters	l
qt	quarts	0.95	liters	l
gal	gallons	3.8	liters	l
ft^3	cubic feet	0.03	cubic meters	m^3
yd^3	cubic yards	0.76	cubic meters	m^3
		TEMPERATURE (exact)		
°F	Fahrenheit temperature	5/9 (after subtracting 32)	Celsius temperature	°C

° 1 in = 2.54 (exactly). For other exact conversions and more detailed tables, see NBS Misc. Publ. 286. Units of Weights and Measures. Price $2.25, SD Catalog No. C13.10:286.

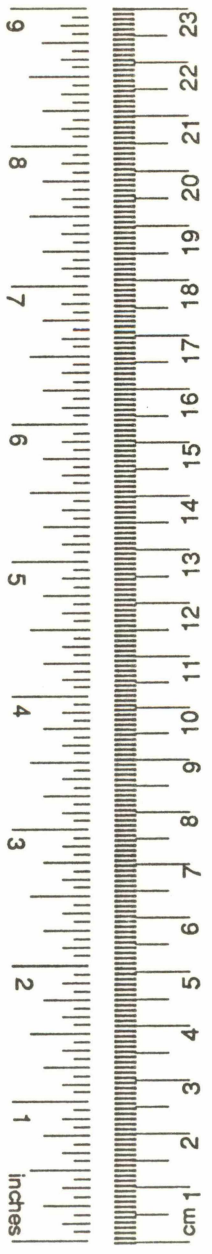

Approximate Conversions from Metric Measures

Symbol	When You Know	Multiply by	To Find	Symbol
		LENGTH		
mm	millimeters	0.04	inches	in
cm	centimeters	0.4	inches	in
m	meters	3.3	feet	ft
m	meters	1.1	yards	yd
km	kilometers	0.6	miles	mi
		AREA		
cm^2	square centimeters	0.16	square inches	in^2
m^2	square meters	1.2	square yards	yd^2
km^2	square kilometers	0.4	square miles	mi^2
ha	hecteres (10,000 m^2)	2.5	acres	
		MASS (weight)		
g	grams	0.035	ounces	oz
kg	kilograms	2.2	pounds	lb
t	tonnes (1000 kg)	1.1	short tons	
		VOLUME		
ml	milliliters	0.03	fluid ounces	fl oz
l	liters	2.1	pints	pt
l	liters	1.06	quarts	qt
l	liters	0.26	gallons	gal
m^3	cubic meters	35	cubic feet	ft^3
m^3	cubic meters	1.3	cubic yards	yd^3
		TEMPERATURE (exact)		
°C	Celsius temperature	9/5 (then add 32	Fahrenheit temperature	°F